

AD-A101 430

GALILEO ELECTRO-OPTICS CORP STURBRIDGE MA  
RADIATION HARD FIBER OPTICS. (U)

MAY 81 R E JAEGER, M ASLAMI

F/6 20/6

F19628-78-C-0099

NL

UNCLASSIFIED

RADC-TR-81-69

1 of 2  
00430  
00430



50  
AD A101430

LEVEL ~~II~~  
12  
RADC-TR-81-69  
Final Technical Report  
May 1981



## RADIATION HARD FIBER OPTICS

Galileo Electro-Optical Corp

Raymond E. Jaeger  
Mohd Aslami

APPROVED FOR PUBLIC RELEASE; DISTRIBUTION UNLIMITED

DTIC  
S JUL 16 1981 D  
H

ROME AIR DEVELOPMENT CENTER  
Air Force Systems Command  
Griffiss Air Force Base, New York 13441

FILE COPY

81 7 15 011

This report has been reviewed by the RADC Public Affairs Office (PA) and is releasable to the National Technical Information Service (NTIS). At NTIS it will be releasable to the general public, including foreign nations.

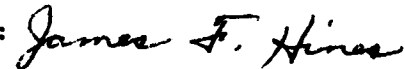
RADC-TR-81-69 has been reviewed and is approved for publication.

APPROVED:



MARTIN G. DREXHAGE  
Project Engineer

APPROVED:



JAMES F. HINES, Major, USAF  
Acting Director  
Solid State Sciences Division

FOR THE COMMANDER:



JOHN P. HUSS  
Acting Chief, Plans Office

If your address has changed or if you wish to be removed from the RADC mailing list, or if the addressee is no longer employed by your organization, please notify RADC (ESM) Hanscom AFB MA 01731. This will assist us in maintaining a current mailing list.

Do not return this copy. Retain or destroy.

## UNCLASSIFIED

SECURITY CLASSIFICATION OF THIS PAGE (When Data Entered)

19. REPORT DOCUMENTATION PAGE		READ INSTRUCTIONS BEFORE COMPLETING FORM
1. REPORT NUMBER <b>18</b> RADC-TR-81-69	2. GOVT ACCESSION NO. <b>10</b> <b>A D-A 102 430</b>	3. RECIPIENT'S CATALOG NUMBER
4. TITLE (and Subtitle) <b>6</b> RADIATION HARD FIBER OPTICS <b>11</b> ≡ ≡ ≡ ≡	5. TYPE OF REPORT & PERIOD COVERED <b>9</b> Final Technical Report <b>14</b> April 1978 - 24 April 1980	
7. AUTHOR(s) <b>10</b> Raymond E. Jaeger Mohd Aslami	6. PERFORMING ORG. REPORT NUMBER <b>13</b> N/A	
9. PERFORMING ORGANIZATION NAME AND ADDRESS <b>16</b> Galileo Electro-Optics Corp. Sturbridge MA 01518	10. PROGRAM ELEMENT, PROJECT, TASK AREA & WORK UNIT NUMBERS <b>15</b> 61102F 01767822 <b>17</b> 78	
11. CONTROLLING OFFICE NAME AND ADDRESS <b>11</b> Deputy for Electronic Technology (RADC/ESM) Hanscom AFB MA 01731	12. REPORT DATE <b>11</b> May 1981	
14. MONITORING AGENCY NAME & ADDRESS (if different from Controlling Office) <b>16</b> Same	13. NUMBER OF PAGES <b>12</b> 98	
15. SECURITY CLASS. (of this report) <b>15a</b> UNCLASSIFIED		
15b. DECLASSIFICATION/DOWNGRADING SCHEDULE		
16. DISTRIBUTION STATEMENT (of this Report)  Approved for public release; distribution unlimited.		
17. DISTRIBUTION STATEMENT (of the abstract entered in Block 20, if different from Report)  Same		
18. SUPPLEMENTARY NOTES RADC Project Engineer: Dr. Martin Drexhage (ESM)		
19. KEY WORDS (Continue on reverse side if necessary and identify by block number) Optical Fiber, Optical Waveguides, Radiation Hardness, Hydroxyl Doping, Cerium Doping, Antimony Doping, Transient Effects, Steady State Effects, Radiation Damage, Glass		
20. ABSTRACT (Continue on reverse side if necessary and identify by block number) A study of radiation-induced absorption in low-loss optical waveguides is reported. Step-index optical fibers were prepared from preforms fabricated by the CVD method. The germanium silicate core glass in the fibers was doped with varying amounts of antimony, cerium, boron, phosphorus and hydroxyl groups. The effects of such variations in the glass chemistry on the radiation induced attenuation of the fibers was evaluated. The transient, steady-state, and temperature-dependent		

UNCLASSIFIED

SECURITY CLASSIFICATION OF THIS PAGE(When Data Entered)

response to radiation was measured. The behavior of fibers containing cerium and antimony indicate that multivalent dopants can be used to modify favorably the radiation response of optical waveguides.

Accession For	
NTIS	GR&I
DTIC TAB	<input type="checkbox"/>
Unannounced	<input type="checkbox"/>
Justification	
By	
Distribution/	
Availability Codes	
Dist	Avail and/or Special
	

UNCLASSIFIED

SECURITY CLASSIFICATION OF THIS PAGE(When Data Entered)

TABLE OF CONTENTS

	<u>PAGE</u>
1.0 <u>INTRODUCTION</u>	1
2.0 <u>EXPERIMENTAL PROCEDURE</u>	4
2.1 Preform Fabrication	4
2.1.1 Hydroxyl Doping	8
2.1.2 Antimony and Cerium Doping	9
2.2 Fiber Drawing	11
2.3 Pre-Irradiation Optical Characterization	12
2.3.1 Attenuation	12
2.3.2 Numerical Aperture	14
2.4 Numerical Aperture	14
2.5 Radiation Response	17
2.5.1 In-Situ Measurement of Induced Loss	17
2.5.2 Transient Induced Loss	20
2.5.3 Induced Loss vs Temperature	21
2.5.4 Radiation Effects on Fiber Strength	26
3.0 <u>RESULTS</u>	28
3.1 Glass Chemistry Effects on Radiation Induced Attenuation	28
3.1.1 Steady-State Response	31
3.1.2 Transient Response	35
3.1.3 Temperature Effects	39
3.1.3.1 Steady-State Results	39
3.1.3.2 Transient Results	46
3.2 Radiation Effect on Fiber Strength	52
3.3 Effect of Drawing Conditions on Radiation Response	52

TABLE OF CONTENTS

	<u>PAGE</u>
4.0 <u>DISCUSSION AND CONCLUSIONS</u>	62
4.1    Compositional and Draw Effects	62
4.2    Temperature Effects	63
5.0 <u>INTERACTIVE PROGRAM</u>	70

APPENDIX A

FINAL REPORT

Period: 24 April 1978 to 24 April 1980

1.0 INTRODUCTION

Of the many studies of radiation induced absorption in optical fibers, few have been reported in which the fibers tested were drawn from preforms prepared with deliberately controlled compositions and fabrication procedures.<sup>1,2,3</sup> There is also a lack of sufficient information regarding radiation response as a function of temperature, although some data has been published.<sup>1,4,5</sup> From a practical point of view, the determination of the temperature dependence of radiation response is of considerable importance in the application of optical fibers under environmental conditions where extreme temperature variations may be encountered. However, some insight into the physical processes involved in the production of induced loss can also be obtained from such measurements.

The process of reducing the radiation induced darkening of glass by the addition of multivalent elements has existed for a number of years.<sup>6,7</sup> The basic concept is the introduction of one or more dopants in suitable redox states such that hole or electron traps are formed that compete with traps intrinsic to the base glass and have absorption bands outside the wavelength range of interest. Although the principle has been well established for standard optical glasses, it has not been proven for the high-purity silicates used in optical fibers.

Another aspect of well controlled experimentation that appears to be lacking in the radiation testing of fibers is the establishment of a firm baseline of reference fibers to which the test results of other fibers can be related. RADC/ES has an ongoing program for the development of radiation tolerant fibers which includes these factors and investigates the radiation responses of optical fibers fabricated under well documented conditions from preform to drawing process. This manuscript is the Final Report on the results obtained under Contract F19628-78-C-0099, covering the period from 24 April 1978 to 23 April 1980.

The major goals of this contract were to study the effect of glass composition and processing on some important characteristics of optical waveguides. The data generated are intended for ultimate use in optimizing the performance of communication fibers in terms of their attenuation, strength, and radiation hardness. Variations in the chemistry of the core glass consisted of antimony, cerium, boron, phosphorous, and hydroxyl doping of a germanium silicate base glass in a step index configuration. All preforms were fabricated using an inside tube CVD process.

The bulk of the work during the contract, was concentrated in three areas: 1) establishing the reproducibility of the preform fabrication process and radiation tests by measuring the radiation response of germanium borosilicate fibers fabricated with no change in process conditions, 2) determining the effect of the various dopants on the

radiation response of the fibers, and 3) measuring the radiation response of Galite 5020 fiber as a function of temperature. Although some preliminary strength measurements have been made, the emphasis has been in the area of radiation effects on glass chemistry. To date, steady-state as well as pulsed ionizing radiation, in the form of x-rays and  $\gamma$ -rays, has been used exclusively.

In order to pursue temperature effects, an environmental chamber was constructed using exclusively low atomic number materials that would minimize perturbation of the dose at the fiber position. In addition, it was capable of maintaining a sample of optical communication fiber at  $-55 \pm 2^{\circ}\text{C}$  or  $150 \pm 2^{\circ}\text{C}$  for up to six hours. Although this change in scope adversely affected the progress toward the development and testing of new glass chemistries having the potential for superior hardness, we recognized the importance of generating meaningful engineering data on commercially available fiber candidates for use in current system.

We present data on the effect of phosphorous, boron, antimony, cerium, and hydroxyl dopants on the radiation hardness of germanium-silicate optical fibers. We also give results of real-time transient and steady-state radiation induced loss measurements performed at  $-55^{\circ}\text{C}$ ,  $+25^{\circ}\text{C}$  and  $125^{\circ}\text{C}$  on a commercial grade fiber candidate intended for application in an airborne optical data buss.

## 2.0 EXPERIMENTAL PROCEDURE

### 2.1 Preform Fabrication

Standard step index preforms were fabricated using the inside-tube vapor oxidation process shown schematically in Figure 1. A thin-walled fused silica reaction tube,\* which serves as a cladding material for the fiber, is supported on both ends in a glassworking lathe. While rotating, it is heated with an oxygen-hydrogen burner which traverses along its length. Electronic grade chemicals ( $SiCl_4$ ,  $GeCl_4$ ,  $POCl_3$ ) are kept in separate containers at controlled temperatures and ultra-pure oxygen is bubbled through these liquids. The amount of chemical vapors entering the reaction tube is controlled using a mass flow control system incorporating a feedback loop to control the desired quantity of oxygen and chloride vapors. Ultra-pure  $BCl_3$  vapors from a pressurized tank are also monitored and controlled by the system, since  $B_2O_3$  can be used as an intermediate cladding or core component. When used in combination with silica as an intermediate cladding, it helps minimize contamination of the core by transition metal and hydroxyl impurities from the fused quartz tube.

The mixture of oxygen and reactants is passed through the fused quartz tube continuously, the heat for the reaction being provided

\*Amersil TO8WG

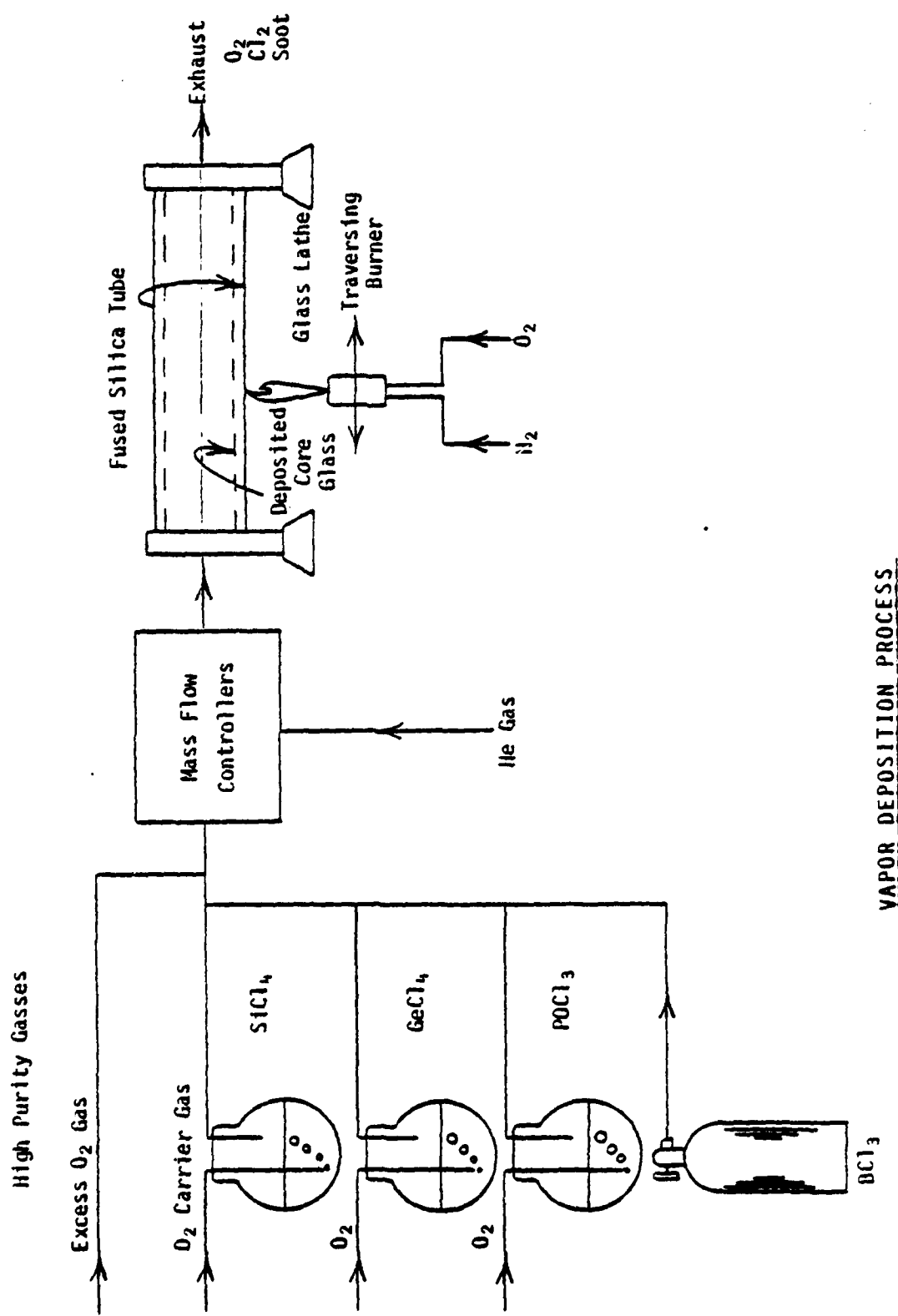


Figure 1

by the traversing burner. The temperature of the tube (1600-1650°C) is continuously monitored and controlled using an optical pyrometer.

In the reaction zone, both the heterogeneous reaction at the tube wall and a homogeneous gas phase reaction take place. The homogeneous reaction produces fine solid particles of oxide glass product, some of which are driven to the tube wall. At the high temperature employed, they are fused to a bubble-free glassy film as the burner passes along the tube. After the desired number of passes have been made, the burner temperature is increased in excess of 1800°C, and the tube is collapsed to form a waveguide preform.

Major emphasis, throughout the program, was placed on control of glass chemistry at the preform fabrication stage. Maintaining composition control, however, was difficult for two reasons. First, the kinetics of the inside-tube CVD reactions are not well known, and second, the effect on these reaction kinetics, due to the presence of unusual dopants, further complicates process control.

The approach finally used was to control the composition of the vapor stream entering the reaction tube. The nominal composition of the germanium silicate base glass was maintained constant at a vapor stream concentration level of  $\approx$  62 mole% silica and  $\approx$  38 mole% germania, assuming complete conversion to the oxides. Dopant levels ranged from 0.2 to 4.0 oxide mole percent in the

gas stream. Slight adjustments in the silica and germania concentrations were made, when necessary, to produce high quality, bubble-free preforms having consistent optical and geometrical characteristics.

For the experiments directed at studying the effects of glass chemistry on radiation response, the fiber numerical aperture was maintained at  $0.2 \pm 0.03$ , and the attenuation at 900 nm was typically  $< 10$  dB/Km. The preform was drawn to a fiber diameter of 125  $\mu\text{m}$  with a 50% core-clad ratio. During the course of the program, the polymer buffer material was upgraded in terms of mechanical isolation properties. At the start of the program a relatively hard buffer was used and resulted in higher spooled, pre-irradiated attenuation. The current buffer has an elastic modulus on the order of  $10^3$  psi, and has significantly reduced the measured attenuation of spooled fiber.

For that portion of the contract concerned with temperature effects in commercial grade fiber, standard Galite 5020 product was used. These fibers have an  $\text{NA} \geq 0.25$  and an attenuation at 900 nm of approximately 5 dB/Km. The fiber OD is 200  $\mu\text{m}$  and has a core diameter of 125  $\mu\text{m}$ .

Although the approach described above for controlling glass chemistry was used throughout the contract, several unsuccessful

attempts were made at analyzing actual dopant concentrations, using X-ray fluorescence and atomic absorption spectroscopy. Indeed, one major thrust of the current contract is to develop composition standards which will be used at minimum, to verify the base glass composition of the fibers. Additional effort will be directed at the analysis of actual dopant concentration.

#### 2.1.1 Hydroxyl Doping

The first series of doping experiments were aimed at increasing the  $\text{OH}^-$  ion concentration in germanium borosilicate preforms to determine its effect on the radiation response of the fiber. The technique used was to bubble oxygen or helium through high purity water as a means of delivering the vapor to the deposition tube. Interaction of  $\text{SiCl}_4$ ,  $\text{GeCl}_4$ , and  $\text{BCl}_3$  vapors with water vapor in the delivery lines was kept to a minimum by placing the water bubbler at the headstock of the lathe and introducing the water vapor at the rotary coupling which is sealed to the intake end of the cladding tube. Even with these precautions, some clogging of the rotary coupling occurred along with seed formation in the preform. By increasing the inner diameter of the process lines, moving a mixing filter which was located in the rotary coupling upstream in the process line, and providing a smoother introduction and mixing of the chemical vapors and water vapor, hydrolysis of the chemicals was kept to a minimum. Another technique attempted was the introduction of hydrogen gas directly into the reactant stream.

### 2.1.2 Antimony and Cerium Doping

Antimony and cerium doping were also undertaken to determine any radiation hardening effects. Unfortunately, no compounds were found with sufficient vapor pressure at room temperature to enable their use in the standard process. Antimony pentachloride, for example, has a vapor pressure of only 1.6 torr at 30°C which is insufficient for conventional processing. At 60-80°C, however, significant vapor pressure is realized, and is nominally the region utilized for our experiments.

Maintaining this temperature in the bubbler and delivery lines required a special system shown schematically in Figure 2. It consists of an Applied Test Systems, Inc. series 2911 test oven to supply the necessary temperature control for the bubbler. The oven was modified by boring three ports in its top to allow the fill line, oxygen bubbling line, and process line access to the quartz bubbler. The entire process line from this liquid delivery system to the traversing burner has to be maintained at a higher temperature than the bubbler in order to prevent the vapors from recondensing. To keep the length of this heated process line to a minimum, the liquid delivery system was located at the headstock of the lathe.

Since the chemical is being introduced at the rotary coupling, a special heating manifold was made to encompass the rotary

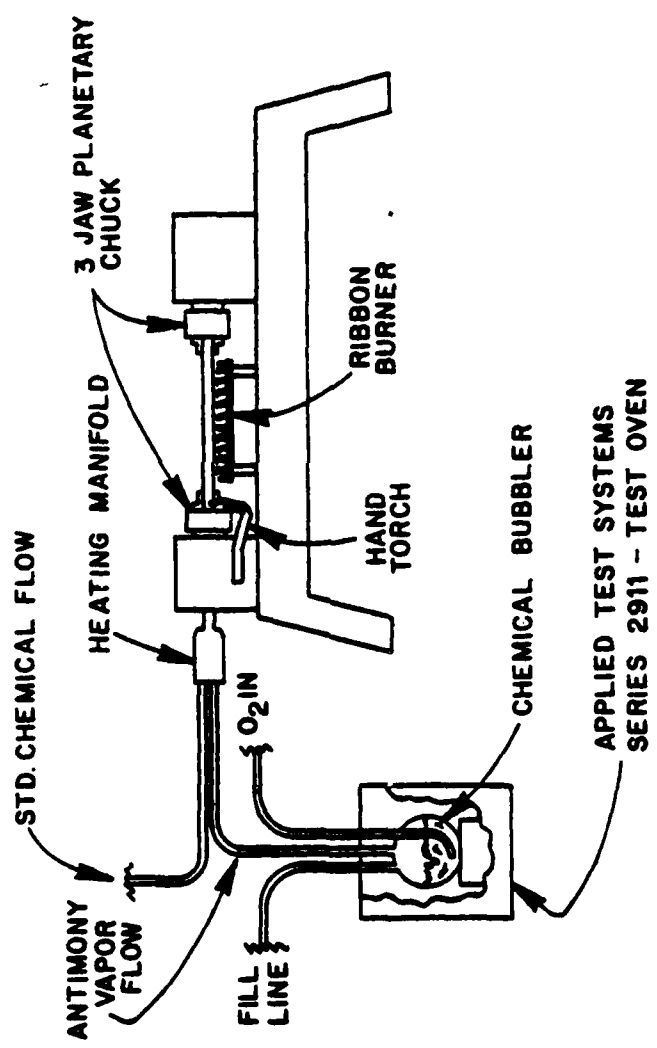


Figure 2

coupling and the intake end of the deposition tube up to the back side of the intake chuck of the lathe. This manifold is maintained at greater than 130°C in order to prevent vapor condensation. The standard Jacob's chuck used on the intake end of the lathe was replaced with a three-jaw planetary chuck which could be heated without loosing its grip on the cladding tube. This change was made after initial antimony doping experiments exhibited vapor condensation as a result of the heat sinking effect of the chuck on the cladding tube. Finally, a ribbon burner was placed under the entire deposition tube to maintain the reactants in vapor form until they entered the reaction zone.

## 2.2 Fiber Drawing

Fibers are drawn using both resistance furnace\* and CO<sub>2</sub> laser\*\* heat sources. The preform diameter is typically 9.5 mm and is drawn into 125  $\mu$ m fiber at a nominal speed of 50 cm/sec. A strength protective polymer coating is applied in-line to the fiber surface and UV cured before it contacts the draw wheels. Approximately 500 meters each of furnace and laser fiber were drawn from a single preform in order to identify effects due solely to the drawing process. The entire length available for testing

\* Centorr Resistance Furnace Model 15, Centorr Associates, Inc.

\*\* CO<sub>2</sub> Laser Model 41, Coherent Radiation.

is then subjected to a 35,000 psi tensile proof test.

### 2.3 Pre-Irradiation Optical Characterization

#### 2.3.1 Attenuation

Optical attenuation is determined by measuring the transmittance of two different lengths of fiber, each of which exceed the steady-state mode distribution length.

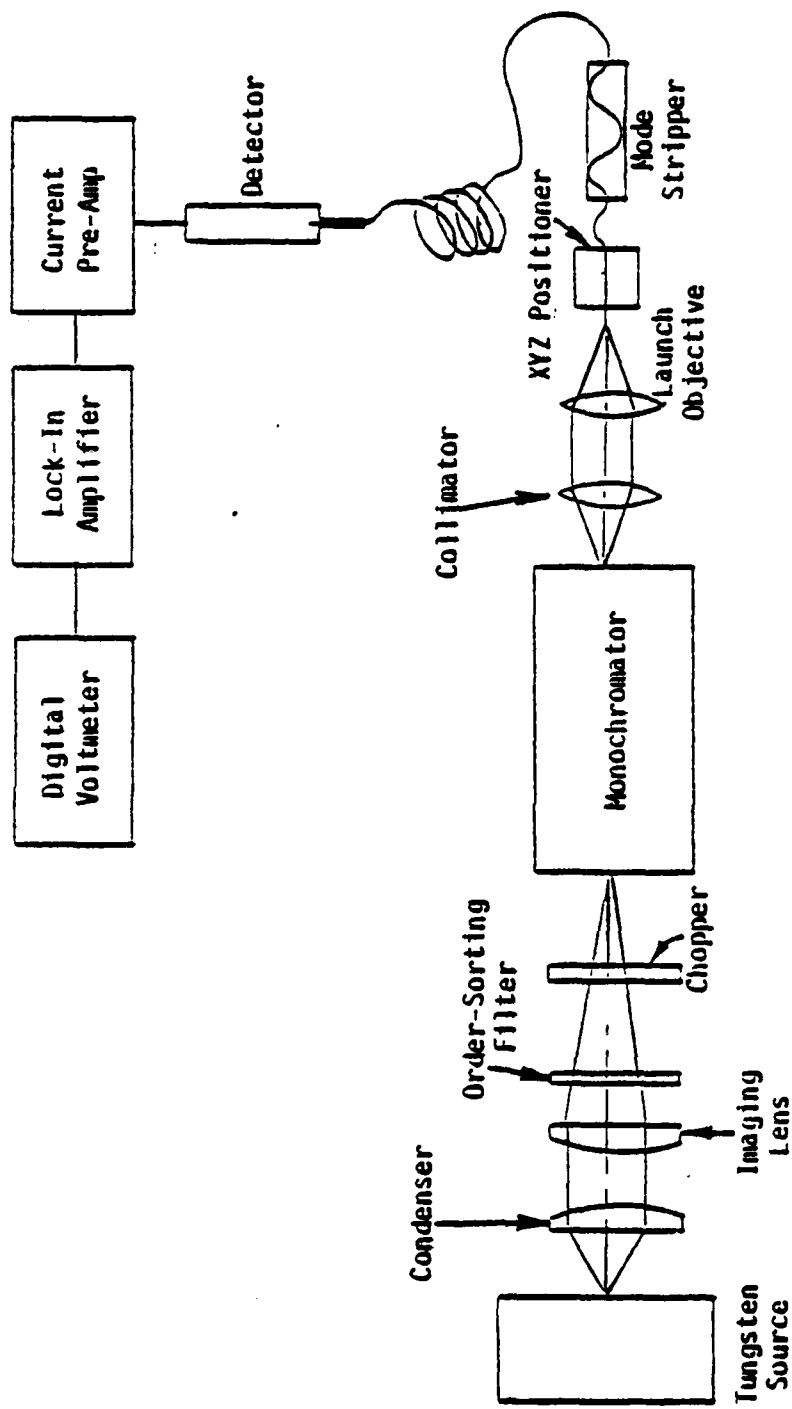
The loss per unit length (L) is calculated by:

$$L \text{ (db/km)} = \frac{10 (\log T_1 - \log T_2)}{(l_2 - l_1)}$$

where  $T_1$  = transmittance of length  $l_1$ .

$T_2$  = transmittance of length  $l_2$ .

A schematic diagram of the spectral attenuation measurement equipment is shown in Figure 3. Fibers and cables are illuminated at the steady-state numerical aperture with a 100W tungsten-halogen source and a stabilized power supply. Spectral attenuation measurements between 0.6  $\mu\text{m}$  and 1.1  $\mu\text{m}$  are accomplished using filters, or a diffraction grating monochromator of the Czerny-Turner configuration, with a bandwidth of 10 nm. Output radiation is detected with a silicon photodiode coupled to a current sensitive pre-amplifier. Measurement of the two lengths of fiber is done with the input end common to both lengths, thus avoiding errors due to differing launch conditions. Effects of differing output



SCHEMATIC DIAGRAM OF SPECTRAL ATTENUATION EQUIPMENT

Figure 3

conditions are minimized by using index-matching fluid at the fiber detector interface and maximizing the output with several end cuts.

#### 2.3.2 Numerical Aperture

The effective numerical aperture of fibers is measured from the far-field radiation pattern using an optical fiber apertometer. A schematic diagram of the apertometer is shown in Figure 4. Input illumination is similar to that used for spectral attenuation measurements. The output end of the illuminated fiber is positioned at the first surface and on-axis to a galvanometer mirror scanner which sweeps the far-field pattern across a point detector. The detector output is electronically integrated and plotted with respect to angle on an X-Y recorder. Effective numerical aperture is defined as the sine of half the angle which encloses 90% of the power emitted from a fiber with length exceeding the steady-state length.

#### 2.4 Fiber Strength

The apparatus used to determine fiber tensile strength is shown in Figure 5. The failure load is measured by a 25 (+ .25 kg Chalitron strain gage mounted on a Unislide\*. The slide mechanism is driven by a variable speed motor which is capable of producing strain rates

\* Unislide Model B4030, Velmex, Inc.

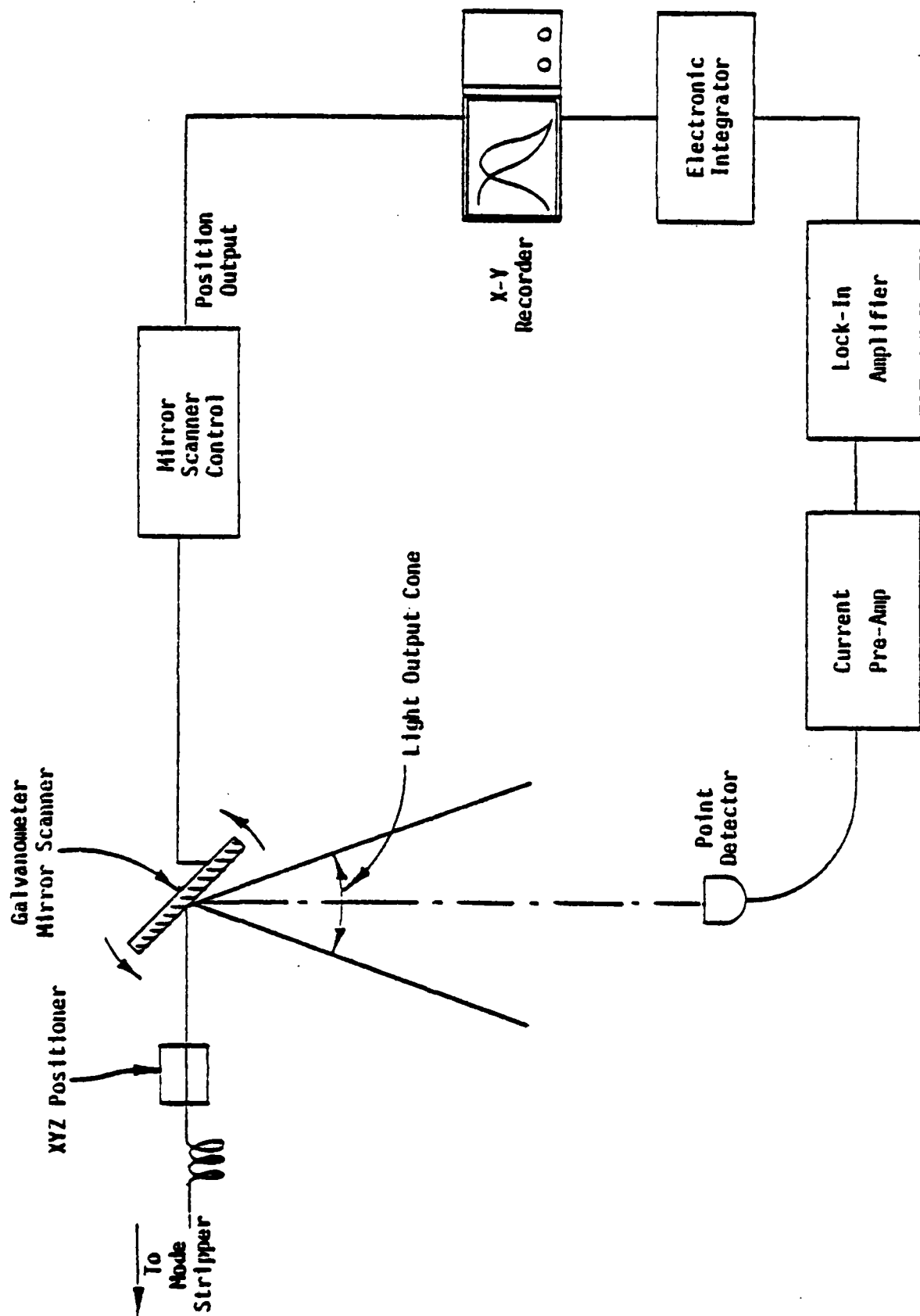


Figure 4

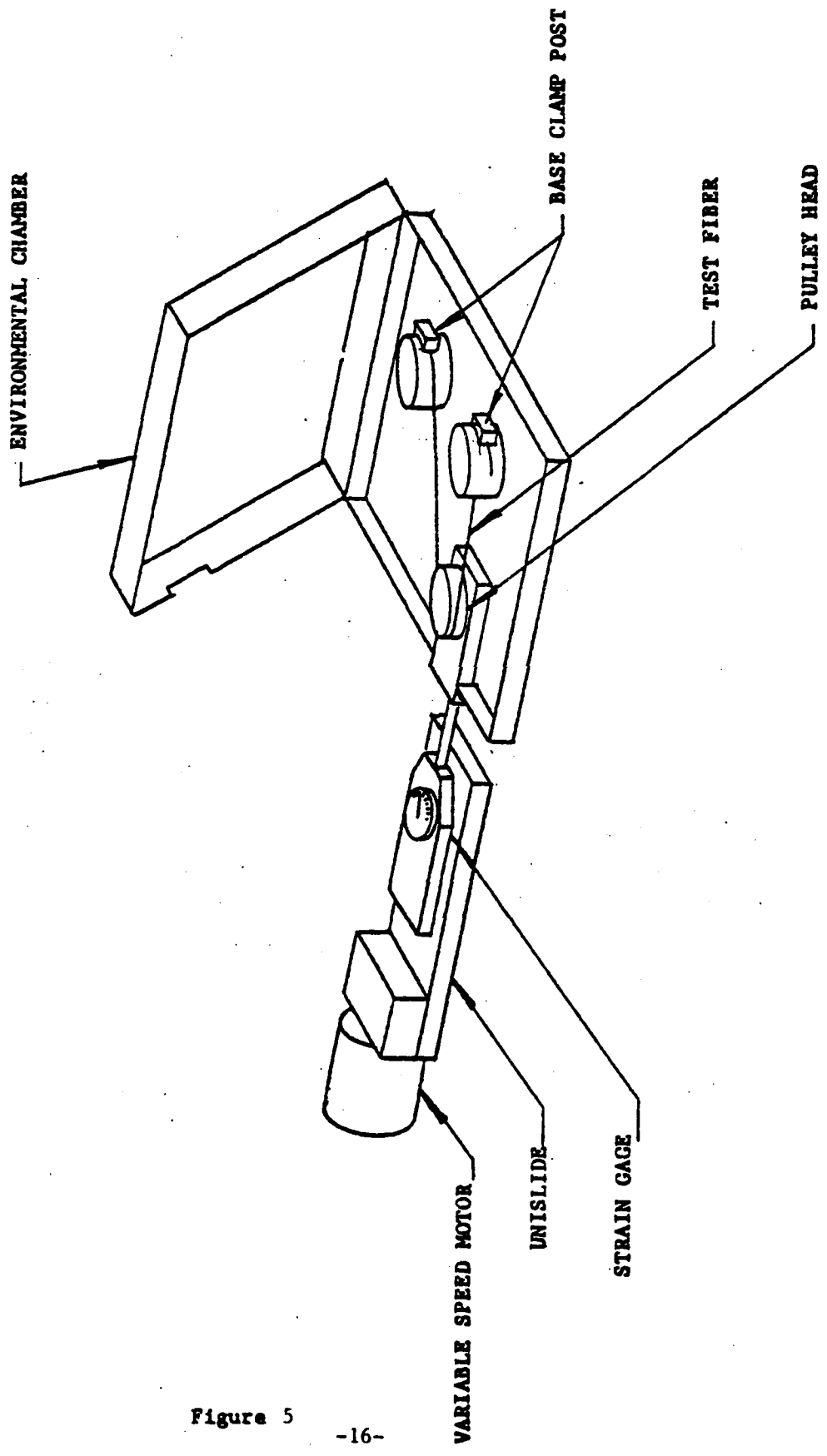


Figure 5

varying over three orders of magnitude from  $.01\% \text{ s}^{-1}$  to  $1\% \text{ s}^{-1}$  ( $\pm 2\%$ ). The test fiber is attached to the base post using a felt padded clamp, then wound 180-degrees around a freely revolving aluminum pulley (4" diameter) which is attached to the strain gage, and is finally terminated by clamping it to the remaining base post. The test gage length achieved with this technique is 1 meter. A minimum of 10 samples are tested, the fracture load recorded, and the fracture end examined. The diameter of the coated and uncoated fiber was measured to  $\pm 1 \mu\text{m}$  using a digital micrometer for only those samples where failure occurred within the gage length (breaks at clamps or pulley were discarded) and these data were used to calculate fracture stress. For a given strain rate, the mean and standard deviation of the fracture strength was calculated.

## 2.5 Radiation Response

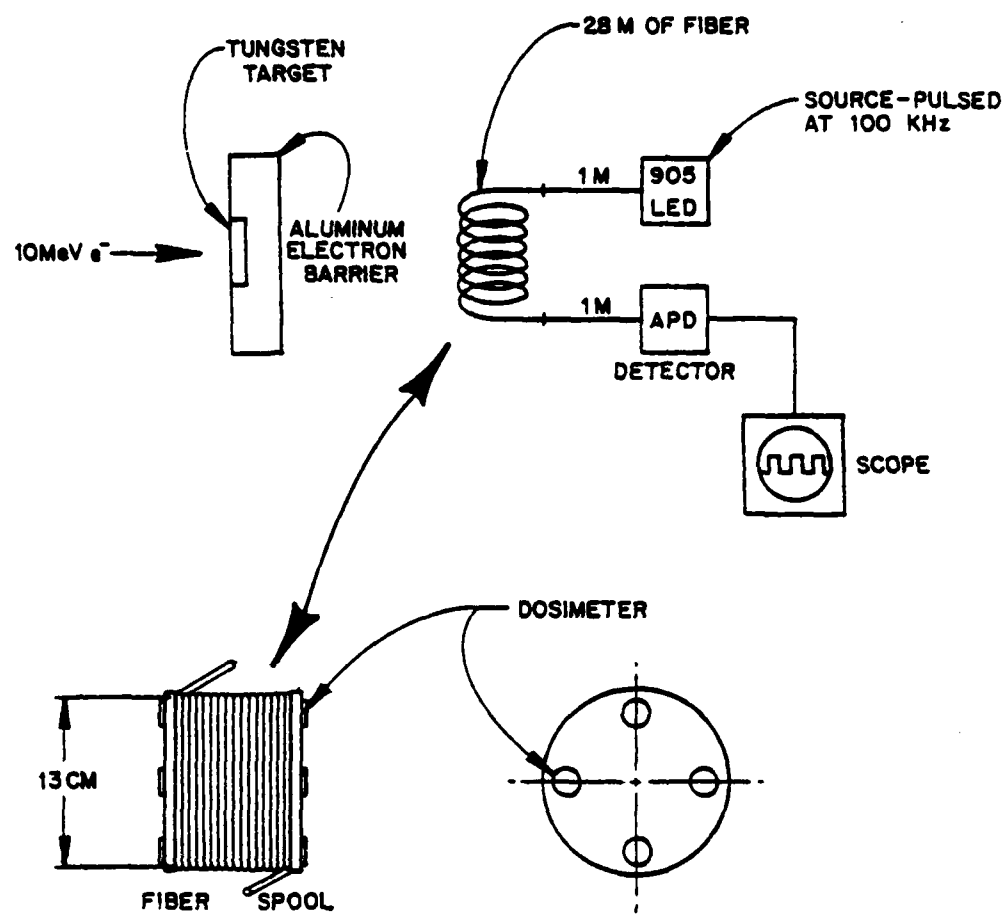
### 2.5.1 In-Situ Measurement of Induced Loss

The in situ measurements on radiation-induced attenuation were carried out by RADC personnel on their linear accelerator. These steady-state irradiations were performed using x-rays, produced by 10 MeV electrons from the RADC linear accelerator (linac) incident on a tungsten target. The linac was set to produce 4.5  $\mu\text{sec}$  wide pulses of electrons and the pulse rate could be varied at will. This made it possible to change the average dose-rate to the fibers instantaneously

during, and without interrupting the irradiation, to test dose-rate effects. At the beginning of the irradiations the linac pulse rate was set for 1 pps. The pulse rate was doubled at intervals during the irradiation. The maximum rate reached during any of the irradiations was 16 pps, giving an average dose-rate range of approximately 1-16 rads/sec.

A schematic of the experimental set-up used for the steady-state irradiations is shown in Figure 6. Twenty five meters of fiber were wound on 13 cm diameter, 1 cm thick reels and positioned relative to the x-ray target to receive approximately one rad per linac pulse. The light source was a 905 nm LED pulsed with 10  $\mu$ sec wide pulses at a rate of 100 kilohertz. The detector was an APD-amplifier module. The source and detector were located out of the direct x-ray beam and were shielded from scattered radiation by lead bricks. The output of the detector was connected to an oscilloscope in the experiment control area which was used to observe and photograph the amplitude of the light pulses transmitted by the fiber during the irradiation. The fibers were irradiated until the transmitted pulse amplitude dropped to half its pre-irradiation value.

Dosimetry for the steady-state irradiations was performed using thermoluminescent dosimeters (TLD's) placed in quadrature around (and on both sides) of the reels and in line with



**RADC/ES**  
**RADIATION MEASUREMENT of OPTICAL**  
**FIBER USING LINAC**

**Figure 6**

the fiber position. The TLD's measured the total dose accumulated by the fiber. During the irradiation, the number of linac pulses accumulated was registered on a counter and the fiber transmission was measured as a function of the number of linac pulses. Following the irradiation the total dose to the fiber as measured by the TLD's was divided by the total number of linac pulses accumulated to obtain an accurate measure of dose per linac pulse. The data was then converted to fiber transmission as a function of dose. The estimated accuracy of the measurements is  $\pm 2$  db/km.

#### 2.5.2 Transient Induced Loss

The transient radiation response measurements were performed using the RADC flash x-ray generator which produces single 20 nanosecond wide x-ray pulses of nominal 2 MeV peak energy. The fibers were exposed to nominal dose rates of  $10^8$  and  $10^9$  rads/sec. The APD module, which had a D.C. to 40 megahertz bandwidth, used for the steady-state irradiations was also used as the detector for these measurements. The LED light source was replaced by a quartz iodide lamp and monochromator set at 905 nm. The fiber lengths (25 meters) and reels were the same as for the steady-state tests. The light source was located in the irradiation area but out of the x-ray beam path. The output end of the fiber being irradiated was coupled to the detector in the experiment control area through a fiber-

optic link. The output of the detector was connected to four oscilloscope inputs to obtain measurements over a time span from less than 50 nanoseconds to 100 milliseconds. The dose-rate received by the fiber was measured by means of a small PIN diode in contact with the fiber on the reel. The estimated accuracy of the measurements for the transient tests is  $\pm$  3 db/km.

#### 2.5.3 Induced Loss vs Temperature

A temperature control chamber, specially designed for use with the RADC/ES radiation facilities, was constructed for these tests. Except for low mass heating and temperature sensing elements, and remote connections located some distance from the fiber position, it is made of all low atomic number materials to prevent perturbation of the radiation fields at the sample position. The walls are double plywood with fiberglass insulation and the sample chamber is aluminum. The chamber is divided by aluminum baffles to one of which is mounted a 900 watt heating element used to attain temperatures up to +150°C. The lower part of the chamber serves as a liquid nitrogen reservoir. The fibers are wound on 13 cm diameter, 1.5 cm thick aluminum reels which mount on the upper end of a moveable aluminum strut. The base of the strut rests on the bottom of the chamber so that it serves as a cold finger when the reservoir is filled with liquid nitrogen. A low-power heating element attached to the strut controls the temperature,

measured by a thermocouple, at the sample position.

Temperatures are maintained to within  $\pm 1^{\circ}\text{C}$  by proportional controllers and thyristor packs mounted in a console which can be located up to 25 meters from the chamber and radiation sources. The console also includes a digital thermometer for continuous temperature monitoring and an automatic liquid nitrogen fill controller which, in conjunction with a 60 liter pressurized Dewar, can maintain the lower temperatures for at least six hours.

Steady-state irradiations were performed using the RADC linear accelerator, which was set to produce electron pulses 4.5  $\mu\text{sec}$  wide at an approximate rate of 5 pps. The fiber, mounted in the temperature control chamber, was positioned relative to the x-ray target so that it received a uniform irradiation of about 0.5 rads per (linac) pulse. The ends of the fiber were brought out of the chamber and coupled to an 850 nm LED source operated in continuous mode and a PIN photodiode-amplifier detector. The source and detector were located out of the direct x-ray beam and shielded from scattered radiation by two inches of lead. The output of the detector was fed to the experimental control area by coaxial cable and connected to a digital voltmeter and chart recorder for continuous observation of the fiber transmission. A pulse counter was used to measure the

accumulated number of linac pulses. The voltmeter reading was recorded as a function of total linac pulses at frequent intervals while the chart recorder provided a continuous reading of the detector output as a function of time. Following the irradiation, the chart recorder was used to monitor recovery of the induced loss.

Dosimetry was performed as in the room temperature measurements, using thermo-luminescent dosimeters (TLD's) mounted in quadrature on each side of the fiber reel at the fiber position. The TLD's measured the total dose to which the fiber was exposed during the irradiation, and as described above, the data taken in terms of induced loss as a function of accumulated linac pulses was then converted to loss as a function of dose.

Because the linac is a pulsed radiation source, a set of irradiations was also performed on one of the fibers using the RADC Co-60 source to check the validity of using the linac for steady-state tests. The arrangement was similar to that using the linac except that the source and detector were located outside the cobalt cell and an ionization chamber was used to monitor accumulated dose. The ionization chamber could not be operated at the temperature extremes in these tests, so it was located outside and adjacent to the temperature control chamber in a position where it received

approximately the same exposure as the fiber. The chamber readout was set to indicate accumulated dose and its output connected to a second pen on the chart recorder so that induced loss and accumulated dose could be measured simultaneously. As with the linac irradiations, TLD's were used as a final calibration of the dose indicated by the ionization chamber since it was not located at the fiber position. These irradiations also provided a calibration of the TLD's at +125°C, a temperature at which they had never before been irradiated.

The transient tests were performed using the RADC flash x-ray generator described in Section 2.5.2. The experimental set up was the same as for the room temperature measurements, with the following exceptions. An 820 nm laser diode operated in continuous mode was used as the light source and a PIN photodiode and 50 megahertz bandwidth amplifier was used as the detector. In addition to the four oscilloscopes used previously, the detector output was connected to an X-Y recorder (with time base) to obtain a time span from less than 50 nanoseconds to over 60 seconds. Dosimetry was performed using a small PIN diode in direct contact with the fiber on the reel, except at +125°C where the PIN could not be operated. In the latter case, dose-rate was estimated from the average of dose-rates measured in preceding "shots" at lower temperatures in the same position relative to the flash x-ray target.

For both the steady-state and transient tests, 75 meter lengths of fiber were irradiated. New lengths of fiber were used for each irradiation with the exception of the transient tests at  $10^8$  rads per second where it was found in preliminary trials that the results of several "shots" on the same fiber were indistinguishable from one another. It was also found that the results of two or three irradiations on the same fiber at  $10^9$  rads per second appeared identical, however, a new section of fiber was used for each irradiation at this level.

Before presenting the radiation test results, it is important to mention significant changes in fiber transmission observed during temperature cycling of unirradiated fiber. The greatest change was observed during warm up. As the fiber was heated from room temperature (about  $20^{\circ}\text{C}$ ) the detected light output from the fiber dropped steadily until at  $+125^{\circ}\text{C}$  it was more than an order of magnitude lower than its starting level. The major cause of this loss in transmission is probably stress produced by expansion of the aluminum reel, even though the fiber was wound on the reel as loosely as possible while maintaining thermal contact. However, other factors such as differential stresses resulting from a non-concentric protective coating, cannot be ruled out.

As the fibers were cooled below room temperature a drop

in signal level was also observed, but not nearly as severe as with increasing temperature, being down on the order of 10 percent at  $-55^{\circ}\text{C}$ . In either case, however, once temperature had been reached signal fluctuations were observed as the temperature cycled around its control point. These fluctuations have an important bearing on the accuracy of the steady-state test results. Without the fluctuations the estimated accuracy is  $\pm 1$  dB/km and at  $-55^{\circ}\text{C}$  and  $+25^{\circ}\text{C}$  the fluctuations change this to  $\pm 2$  dB/km. At  $+125^{\circ}\text{C}$ , as a result of the severe loss in signal, the accuracy is probably reduced to  $\pm 10$  dB/km. For the transient tests estimated accuracy is  $\pm 3$  dB/km based on the readability of oscilloscope photographs. Because of the short time span over which the transient measurements were made, the signal variations should not change this. However the loss of signal at  $+125^{\circ}\text{C}$  probably reduces the accuracy to  $\pm 6$  dB/km due to the decrease in signal to noise ratio.

#### 2.5.4 Radiation Effects on Fiber Strength

Initial experiments to determine radiation effects on fiber strength used fiber wound onto 2.5 cm. diameter glass filled Delrin mandrels according to the following procedure. A mandrel was mounted onto a variable speed spooling device, one end of fifty meters of fiber was secured using tape and the fiber was wound in a tight lay under constant tension

(total bend stress = 75,000 psi). The lay was regulated by controlling the spool speed while the tension was controlled by adjusting the tightness of a felt clamp through which the fiber passed. The tension was monitored using a Schmidt (20 to 300 gm) hand held tensile gage. The end of the fiber was also secured using tape and the mandrel was subsequently bagged in heavy plastic to prevent environmental contamination. The prestressed and packaged in this manner, were irradiated with gamma rays in the RADC Cobalt 60 Cell. The dose rate was 3 Mrads/hr. and the total integrated dose was  $7.5 \times 10^7$  rads.

### 3.0 RESULTS

#### 3.1 Glass Chemistry Effects on Radiation Induced Attenuation

When this contract was initiated, there were two predominant choices of glass chemistry available to commercial manufacturers of multi-mode fiber. These were pure silica clad waveguides having core base glass compositions of germanium silicate doped with either boron or phosphorus. The trend in industry at that time was in the direction of phosphorus doped material, to achieve higher numerical apertures (>0.2), improved thermal expansion match, and better fining characteristics.

At the same time, however, preliminary data on radiation response indicated higher steady-state induced loss in the phosphorus containing material. <sup>(8,9)</sup> It was for this reason,

that we selected the germanium borosilicate chemistry for our reference fiber. The nominal vapor composition of the core in mole percent, assuming 100% conversion to the oxides during deposition, was 61.4 SiO<sub>2</sub>, 37.2 GeO<sub>2</sub> and 1.4 B<sub>2</sub>O<sub>3</sub>.

Step index fibers were drawn from these preforms with 125 $\mu$ m OD and 50% core/clad ratios.

Several reference fibers were prepared and tested at intervals throughout the program to verify control of both the fiber

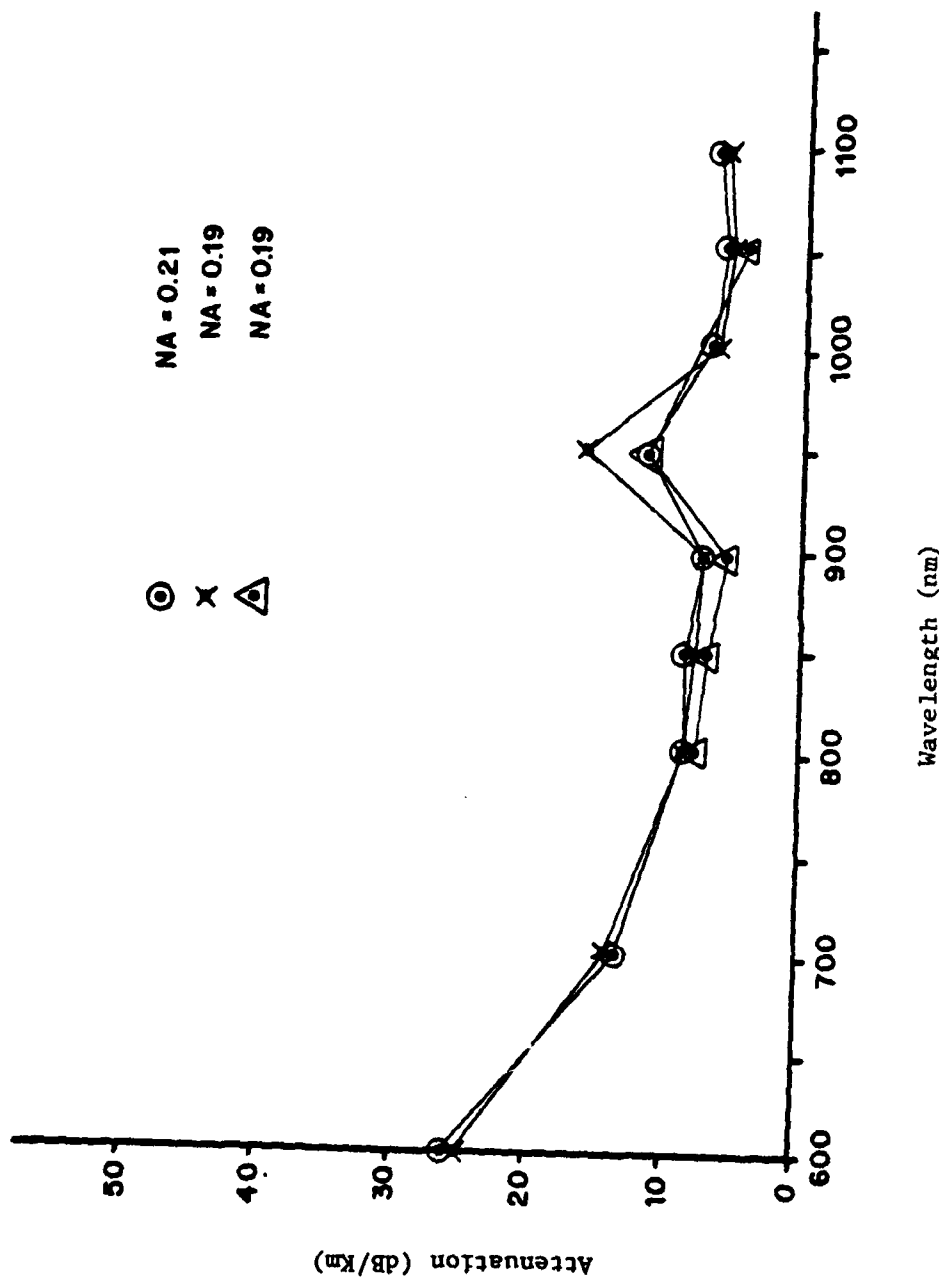


Figure 7

TABLE 1  
**FIBER COMPOSITIONS, OPTICAL PROPERTIES AND RADIATION RESPONSE**

Oxide Mole % in Vapor Stream			OH Conc. (ppm)	NA	Pre-ir radiated Attenuation @ 900mm (db/km)	Radiation Response db/km/krad
Si	Ge	B				
61.4	37.2	1.4	5	0.19	6.2	2.83
61.4	37.2	1.4	5	0.21	5.8	2.72
61.4	37.2	1.4	7	0.19	7.5	2.36 (2.35)*
61.4	37.2	1.4	20	0.26	12.6	3.26
61.4	37.2	1.4	30	0.20	8.5	2.24

\*Remeasured on a different section of fiber from the same preform.

preparation process and the radiation test procedures. Pre-irradiated results of NA and attenuation measurements on 3 such reference fibers are given in Figure 7. All reference fibers (total of 5) were tested for their real-time responses to steady-state radiation in order to establish a baseline for the study of dopant effects. The average rate of induced loss, for a total of 5 fibers measured, was  $2.3 \pm 0.4$  db/km/krad. Both the pre-irradiated optical characteristics and the radiation response, therefore, indicate good process control and test procedures.

### 3.1.1 Steady-State Response

The effect of hydroxyl doping on the radiation response of the base glass composition was determined on 5 fibers containing varying amounts of hydroxyl ions. Referring to Table 1, however, the addition of hydroxyl ions to a germanium borosilicate core glass appears to have no effect on the radiation response of fiber in the range of 5 to 30 ppm OH.

In addition to the hydroxyl experiments, preforms were prepared with various other dopants in the germanium silicate base glass. These compounds were added to the vapor stream in place of, or in addition to the boron, and included antimony, phosphorous, and/or cerium.

TABLE 2  
FIBER COMPOSITIONS AND OPTICAL PROPERTIES

Oxide Mole % in Vapor Stream						OH ppm	N.A.	Attenuation at 900 nm dB/km
Si	Ge	B	P	Sb	Ce			
61.4	37.2	1.4	-	--	--	8	0.17	8.3
65.9	33.9	-	0.2	--	--	3	0.19	7.9
61.3	37.7	0.9	0.2	--	--	6	0.23	7.2
61.3	36.5	1.4	--	0.8	--	13	0.18	6.8
61.7	37.4	-	0.2	0.8	--	2	0.21	5.3
61.1	37.6	0.9	--	--	0.5	5	0.18	5.7

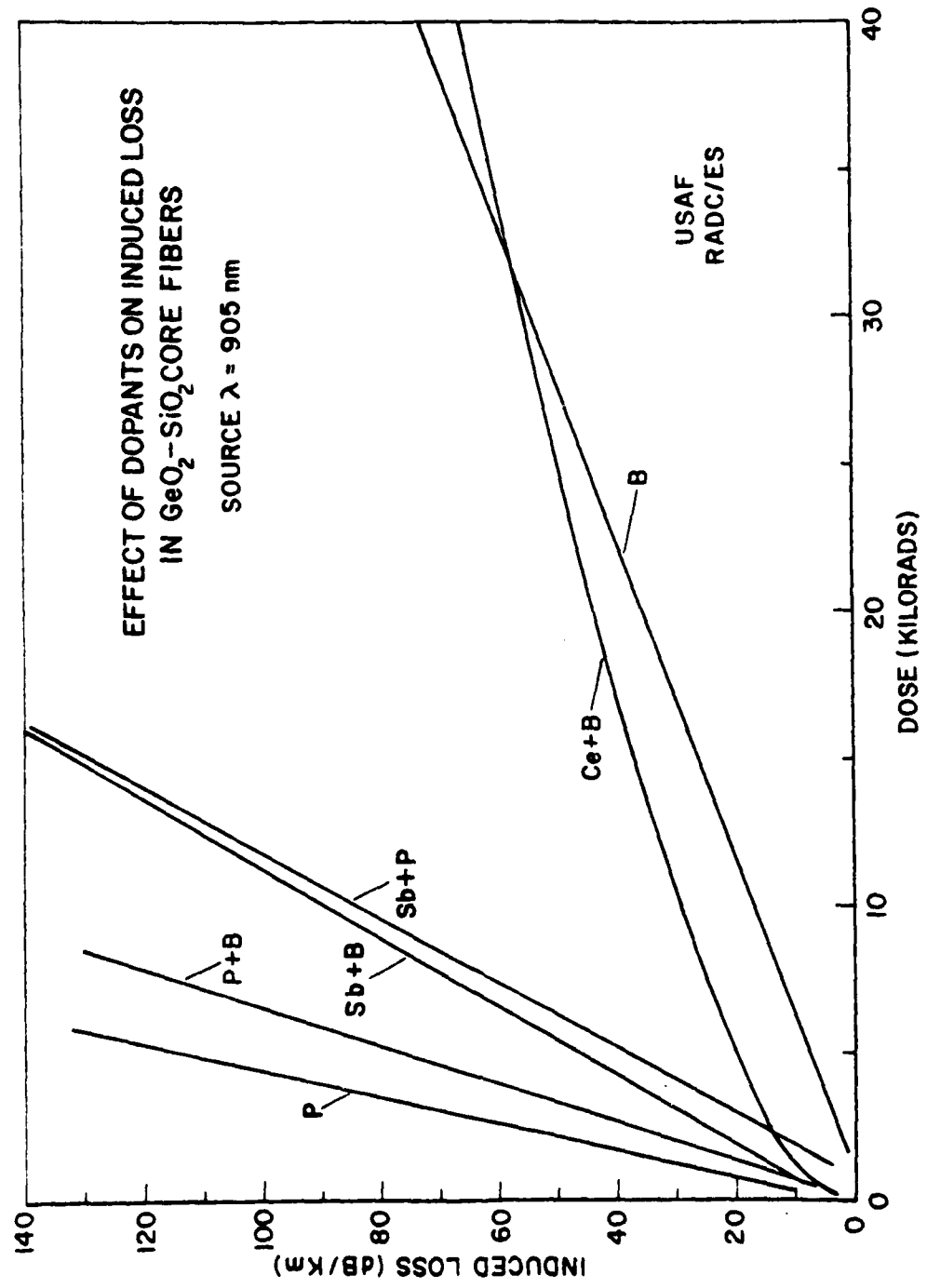


Figure 8  
-33-

Table 2 lists the compositions and optical properties of six fibers containing these dopants. Figure 8 presents data on the radiation response of the different glass chemistries. Actual data points have been omitted for the sake of clarity. In practice, a measurement was taken for every 1-2 db/km change in attenuation. These results were published in the Spring of 1980 as in Appendix A.

Neglecting small deviations (which could have been instrumental in origin) below about 2 kilorads, all of the fibers tested, except the one doped with cerium and boron, showed a very linear induced loss as a function of dose over the range of doses used in the steady-state irradiations. No change in this linearity were observed as the dose-rates were changed.

The rate of induced loss with dose increased by approximately a factor of 4 over that of the baseline fiber when antimony was added to the vapor stream and by about a factor of 7 when phosphorous was added. The substitution of phosphorous for boron increased the rate of induced loss by a factor of 10. This result is consistent with other published data on similar compositions prepared by an outside CVD technique. (2)

Doping with a combination of antimony and phosphorous shows nearly the same result as that obtained with the antimony-boron doped fiber. The data for the fiber doped with cerium

and boron shows a continuously decreasing rate of induced loss with increasing dose, starting at about 6 times, and ending at about 1/2, that of the baseline fiber. The origin of this behavior is discussed in Section 4.1.

### 3.1.2 Transient Response

In the transient tests, the fibers exhibited fluorescent pulses of different intensities and duration. This resulted in overloading the detector, and in some cases, inhibited the ability to measure the transient loss at very short times after the pulse ( $<1\mu$  sec). The phenomenon of Cerenkov radiation can explain a short pulse width fluorescence which would be created in all optical fibers. The effect is described as an electromagnetic shock wave (emission of light) produced when a particle travels through a transparent medium at a speed exceeding the velocity of light in the medium<sup>(10)</sup>. This phenomenon would create a fluorescence pulse width directly related to the length of the fiber tested and such a correlation has been verified.

Coupled with Cerenkov radiation are the fluorescence characteristics of the phosphorous and antimony which can further inhibit transient loss measurement. These

effects can be measured by observing the emitted light without transmitting a signal through the fiber. This gives a baseline magnitude for the fluorescence pulse which can be subtracted from the experimental data to yield the transient loss in the fiber. The detector overload appeared as broadening of the pulse for up to 200 nanoseconds at the  $10^8$  rad/sec level and up to 600 nanoseconds at the  $10^9$  rad/sec level. This prevented loss measurements at times shorter than these.

At  $10^8$  rads/sec none of the fibers doped with phosphorous showed any detectable induced loss. For the others, the induced losses were too small to make meaningful measurements from the oscilloscope photographs. Figure 9 shows the induced losses, at the nominal  $10^9$  rads/sec level (actual dose-rate  $1.7 \times 10^9$  rads/sec) as a function of time over part of the time-span covered by the measurements. The actual measured losses have been divided by dose-rate in units of  $10^8$  rads/sec in figure 2 (normalized induced loss) for better comparison of results obtained for the different fibers. This is necessary because the output of the flash x-ray generator can vary by about 10% from pulse to pulse. No induced loss was observed for the fibers doped with phosphorous

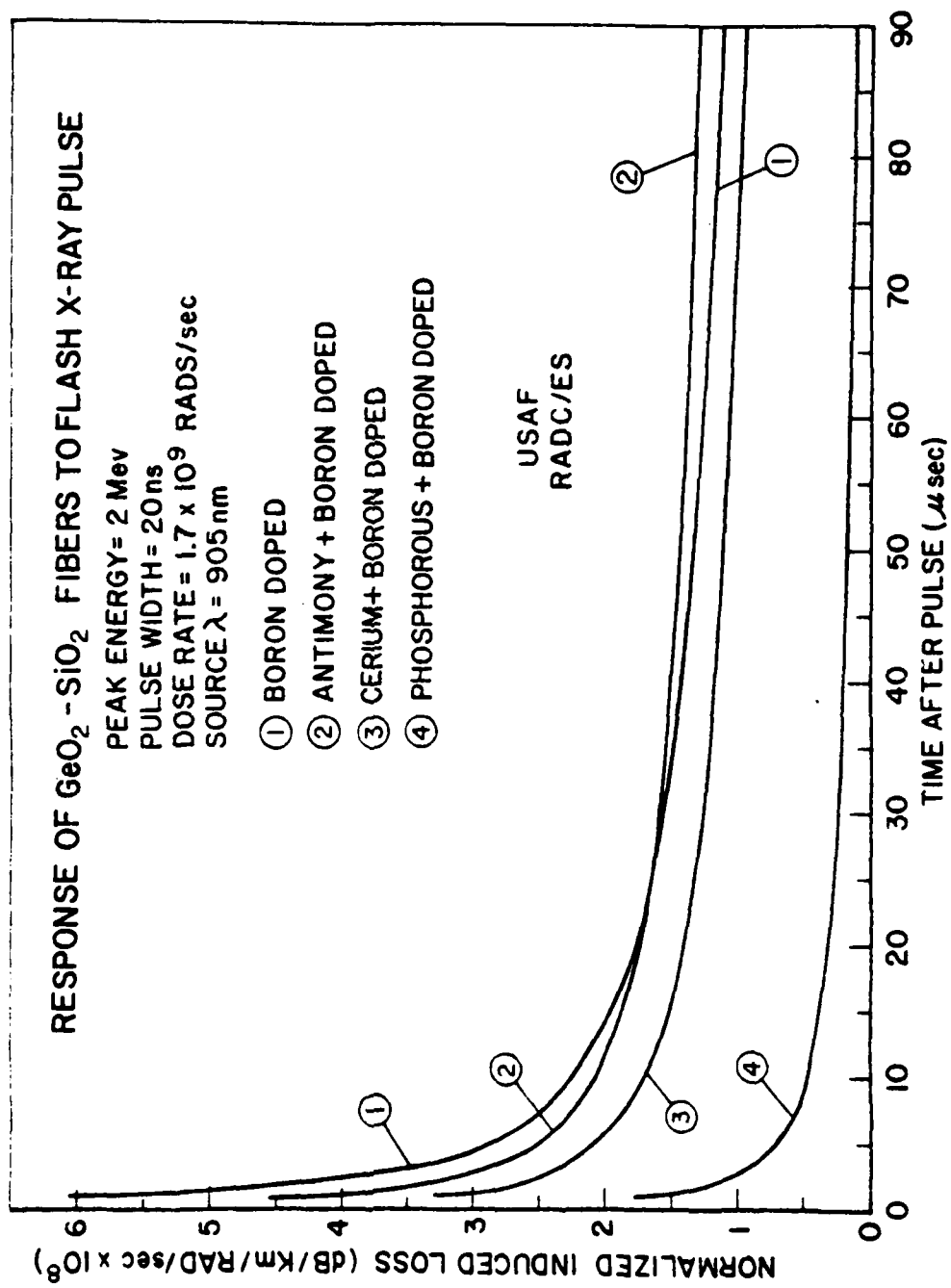


Figure 9  
 -37-

only and antimony plus phosphorous.

The antimony and boron doped fiber appears to show less induced loss than the boron doped fiber. However, there was an indication of a long (at least one microsecond) duration fluorescence generated in that fiber which could cause the measured loss to be less than the actual unduced loss. The generation of this fluorescence was confirmed by tests of two other fibers doped with 2.5% and 4% antimony. For these fibers the fluorescence was evident for 200 and 600 microseconds, respectively, with no light input to the fibers. No long-term fluorescence was observed for the cerium plus boron or phosphorous plus boron doped fibers. Both show lower induced loss than straight boron doped fiber, but have a slightly lower boron concentration in the gas stream. For all the fibers tested under transient radiation the induced losses became undetectable within 100 milliseconds.

### 3.1.3 Temperature Effects

Real-time transient and steady-state radiation induced loss measurements were performed at  $-55^{\circ}\text{C}$ ,  $+25^{\circ}\text{C}$ , and  $+125^{\circ}\text{C}$  on a commercial grade fiber (Galite 5020). This particular product is a prime candidate for use in a military air-borne data buss. The results described below were published as in Appendix B.

The fiber has a germanium phosphosilicate core with a core/clad ratio of 125/200  $\mu\text{m}$  and a numerical aperture of 0.25  $\pm 0.01$ . Unjacketed versions of the fiber were specially fabricated for the tests and measurements were performed on fibers drawn from two preforms. For reference purposes the fibers are designated WP-2 and WP-6, with WP-6 having a higher numerical aperture of 0.26, versus 0.25 for WP-2. This may be the result of a slightly higher germanium concentration in the core of WP-6, but obviously does not place the fiber outside the normal performance specification. Indeed the differences may be considered typical of variations that could occur in normal commercial production. All tests were performed on lengths of fiber taken from a single draw in order to avoid any ambiguities in test results that might be caused by differences between preforms or drawing processes.

#### 3.1.3.1 Steady-State Results

Figure 10 shows the steady-state induced loss as a function of dose measured for fiber WP-2 at  $-55^{\circ}\text{C}$ ,

RESPONSE TO 10 Mev LINAC X-RAYS  
FIBER: WP-2

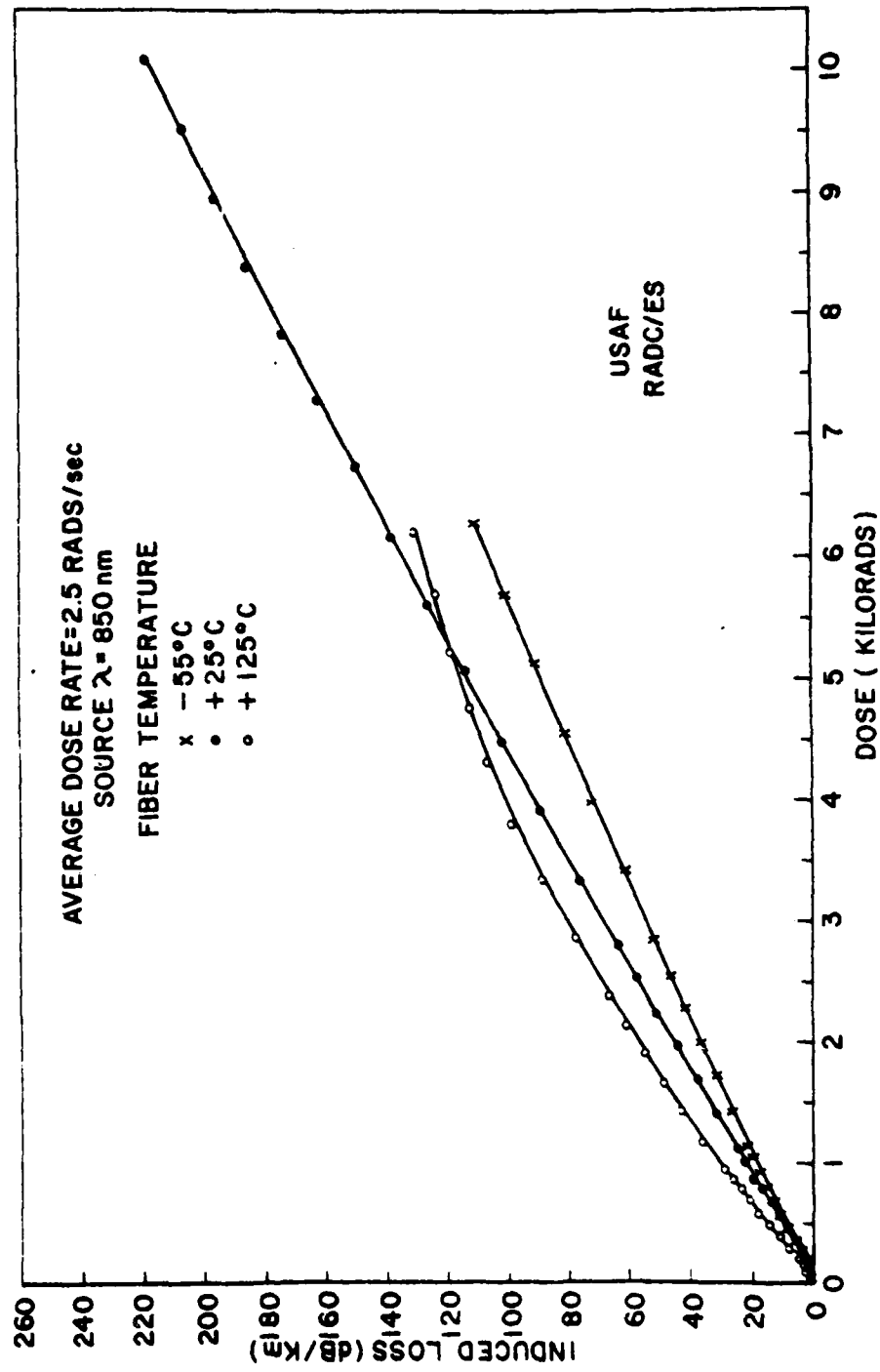


Figure 10

+25°C and +125°C. Although it was intended to irradiate all the test fibers to 10 Krads, the data at -55°C and +125°C ends at just over 6 Krads. This was due to temporary failure of the linac, and because the fibers had received sufficient dose for purposes of the tests, the irradiation was stopped in order to obtain data on the recovery of induced loss following continuous irradiation. The interesting features of this data are the increasing rate of induced loss with temperature and the significant change in slope with increasing dose at +125°C.

Figure 11 shows the recovery of induced loss, expressed as a fraction of the loss at the end of irradiation, for this fiber. There is significant recovery only at +125°C. At -55°C, recovery could be followed only for 5 hours due to depletion of the liquid nitrogen. An observation to be noted, however, was the fact that as the temperature increased from -55°C, the loss increased until at +25°C it was 1.2 times the loss at the end of irradiation.

Figure 12 shows the results of the steady-state irradiations of fiber WP-6. The rates of induced loss are significantly less than those for fiber WP-2. The data taken at +125°C does not follow the trend

RECOVERY OF RADIATION INDUCED LOSS  
FIBER: WP-2

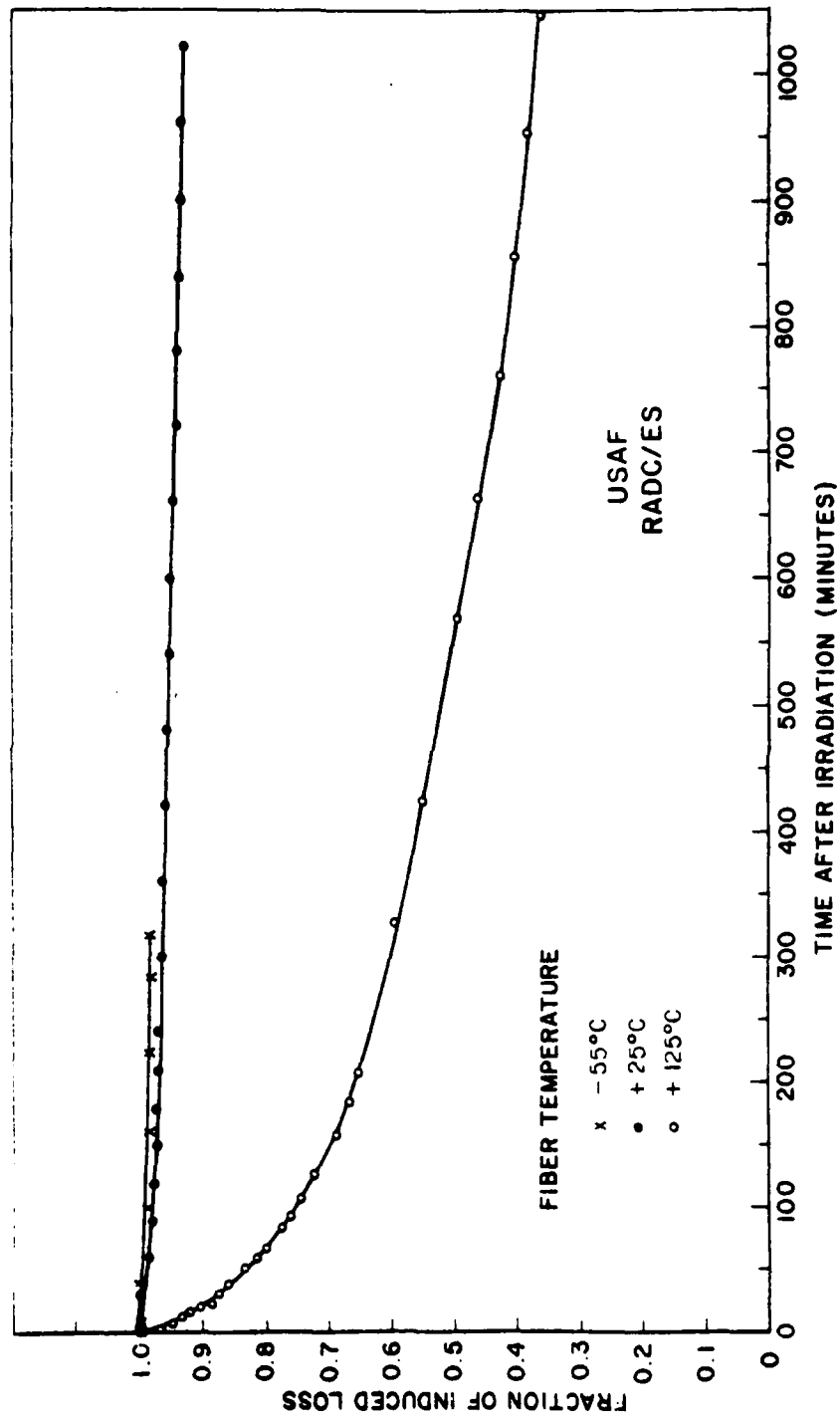


Figure 11  
-42-

RESPONSE TO 10 Mev LINAC X-RAYS  
FIBER: WP-6

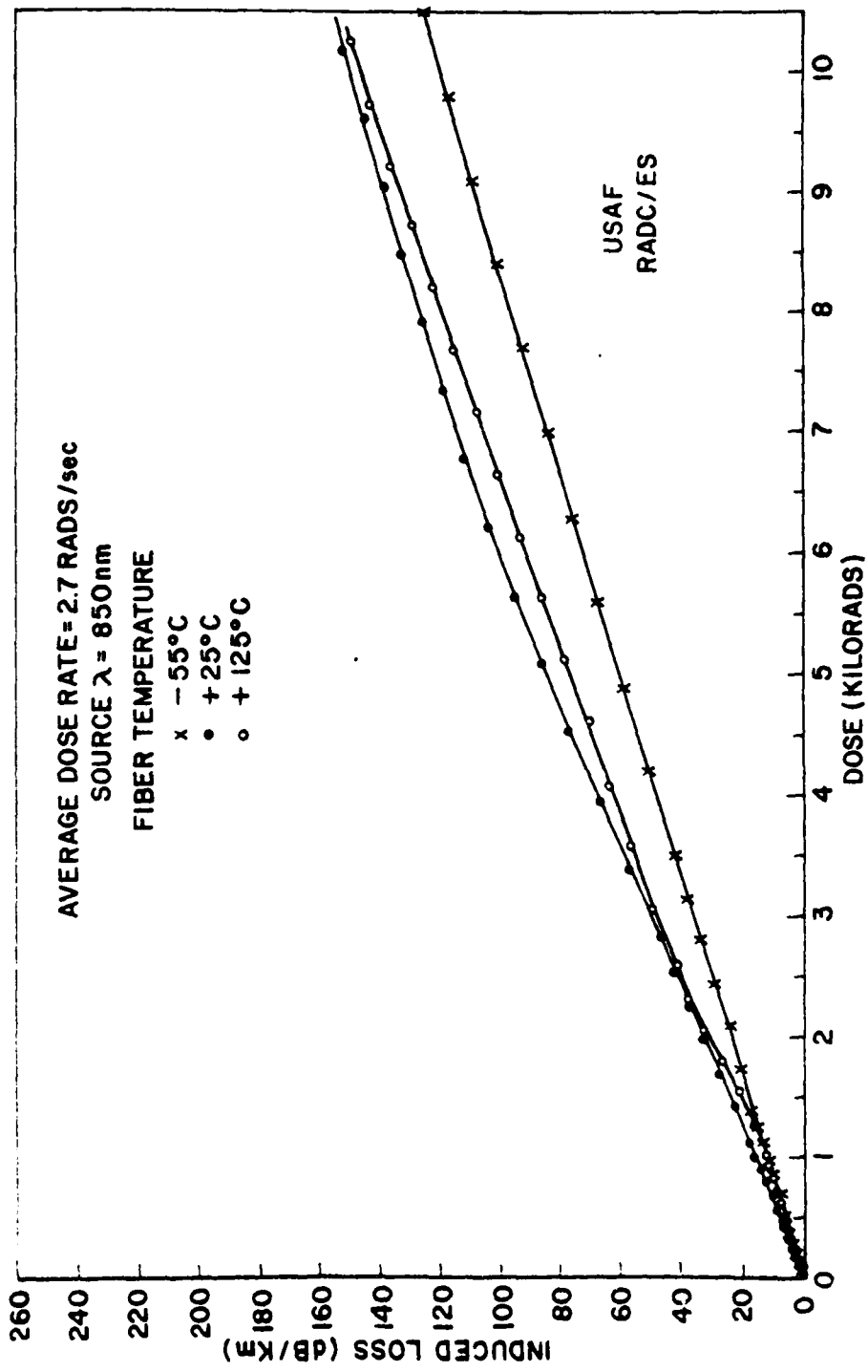


Figure 12

of increasing rate of induced loss with increasing temperature, nor does it show the significant change in slope observed with WP-2. This is probably due to a small temperature excursion near the beginning of the irradiation which may be indicated by the slightly concave portion of the plot near 1 Kilorad. A second fiber irradiated at 125°C did exhibit response consistent with the WP-2 data. We do not report it here, however, because of a malfunction in the linac during the test, which resulted in an unexpected decrease in the dose per pulse.

Instead, another complete set of data was taken using the RADC cobalt 60 cell. These experiments, therefore, served the dual purpose of checking the anomalous behavior of WP-6 at high temperatures, as well as confirming the validity of using the linac for steady-state tests. Figure 13 shows the results of the steady-state Cobalt 60 irradiations of fiber WP-6. The consistent increase in rate of induced loss with increasing temperature, not seen in the linac data, is clear in this case. Comparison with the linac data shows that the data taken at -55°C are essentially identical and the data at +25°C are very nearly the same. The difference in the data at +125°C is probably due to the high sensitivity of

RESPONSE TO Co-60 RADIATION  
FIBER: WP-6

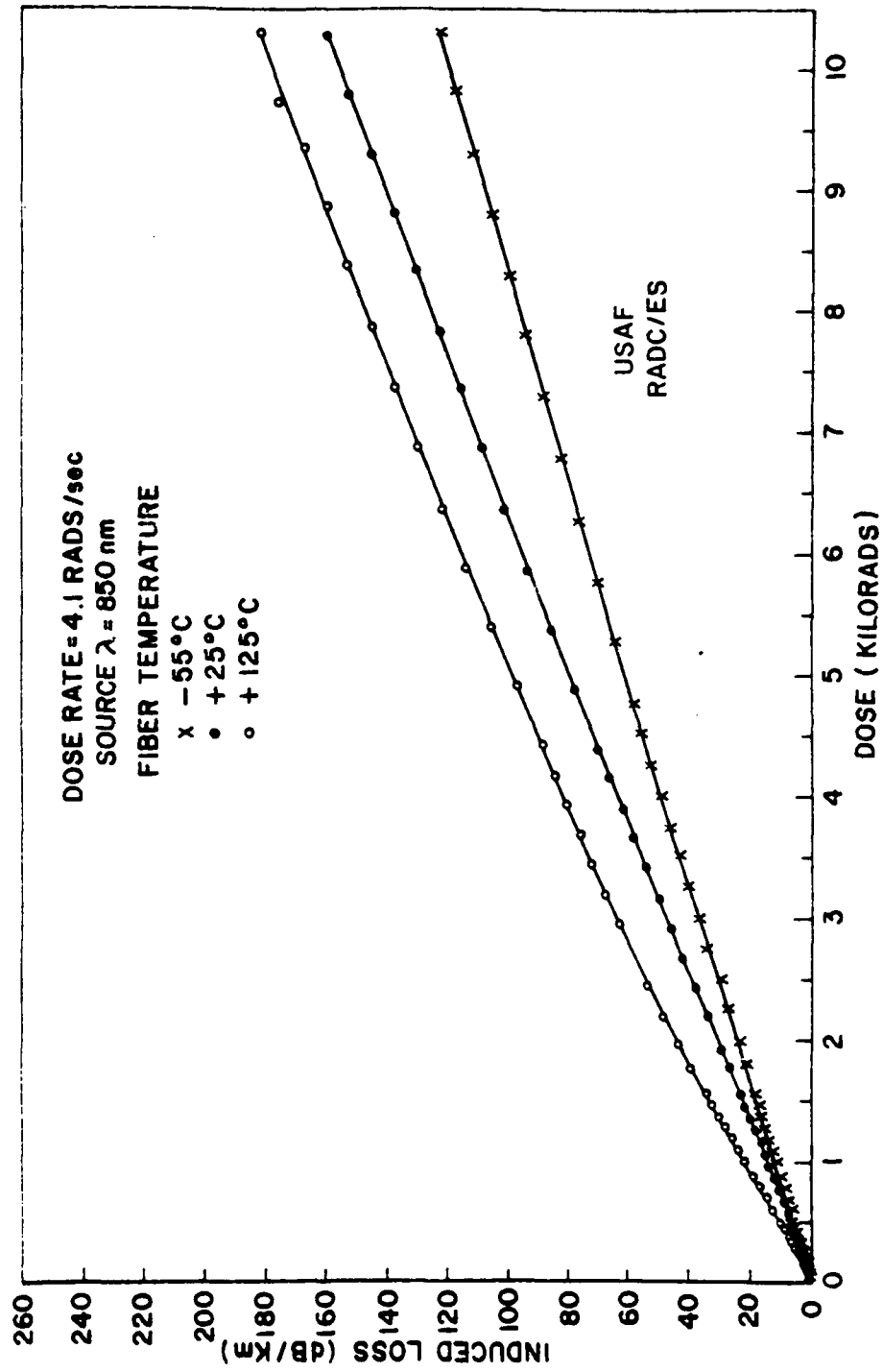


Figure 13

the fiber transmission to small changes in temperature. The control of temperature in the linac irradiation area is somewhat more difficult at +125°C than in the cobalt cell because of a fast moving air stream required to remove ozone during linac operation.

Figure 14 shows the recovery of induced loss following linac irradiation for WP-6. Significant recovery occurs only at +125°C and the rate of recovery is less than for WP-2. Again, when the fiber irradiated at -55°C returned to +25°C the loss increased by a factor of 1.2 times that at the end of irradiation.

### 3.1.3.2 Transient Results

Figure 15 shows the induced loss as a function of time for fiber WP-2 following a 20 nanosecond,  $2 \times 10^9$  rad/sec pulse from the flash x-ray generator. The induced loss has been normalized to actual dose rate and is presented in units of dB/km per  $10^8$  rads/sec. The reason for this normalization is that the flash x-ray does not necessarily produce the same dose from pulse to pulse. Although the variation in output for a given series of irradiations is only about 10 percent, greater variations can occur over

RECOVERY OF RADIATION INDUCED LOSS  
FIBER: WP-6

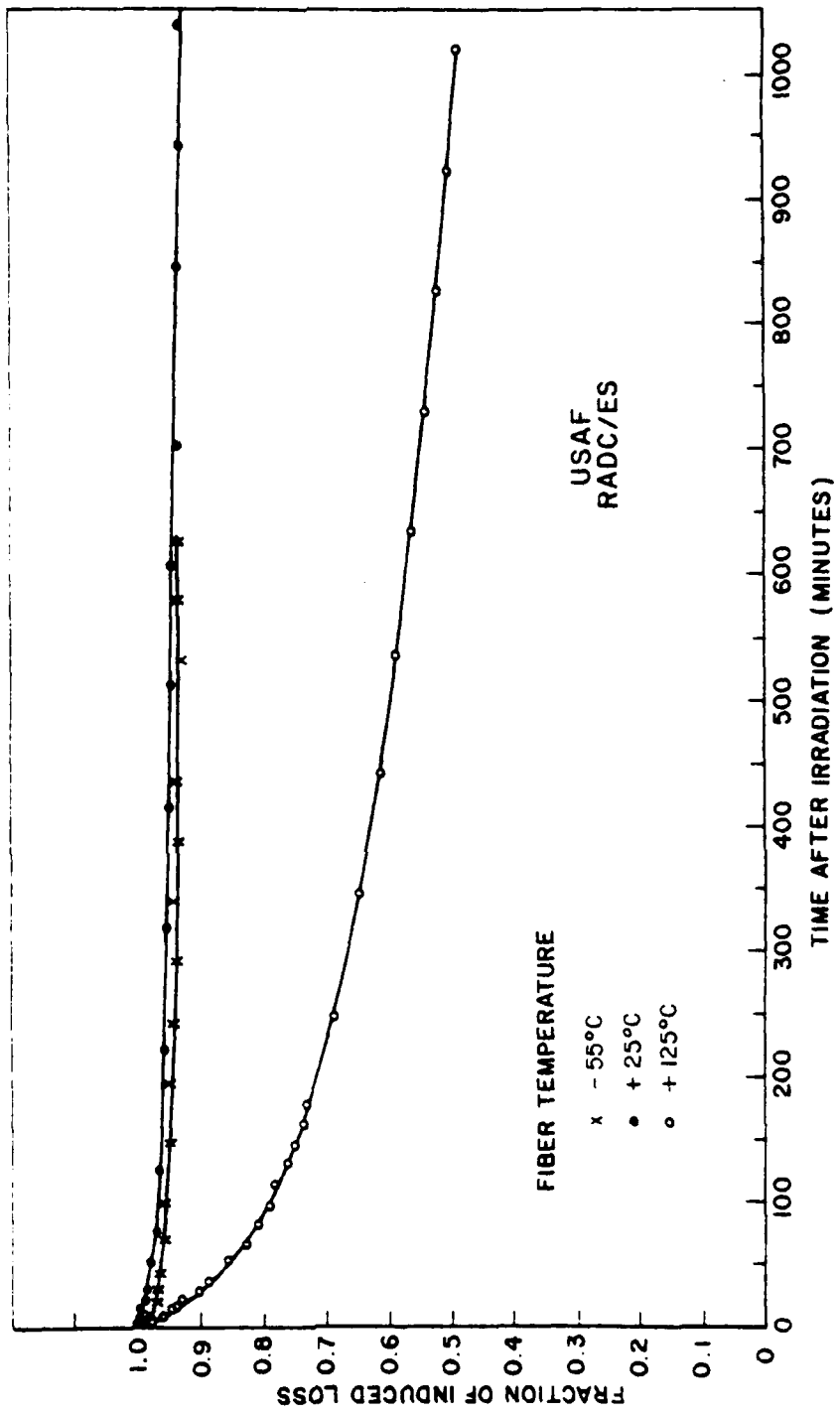


Figure 14

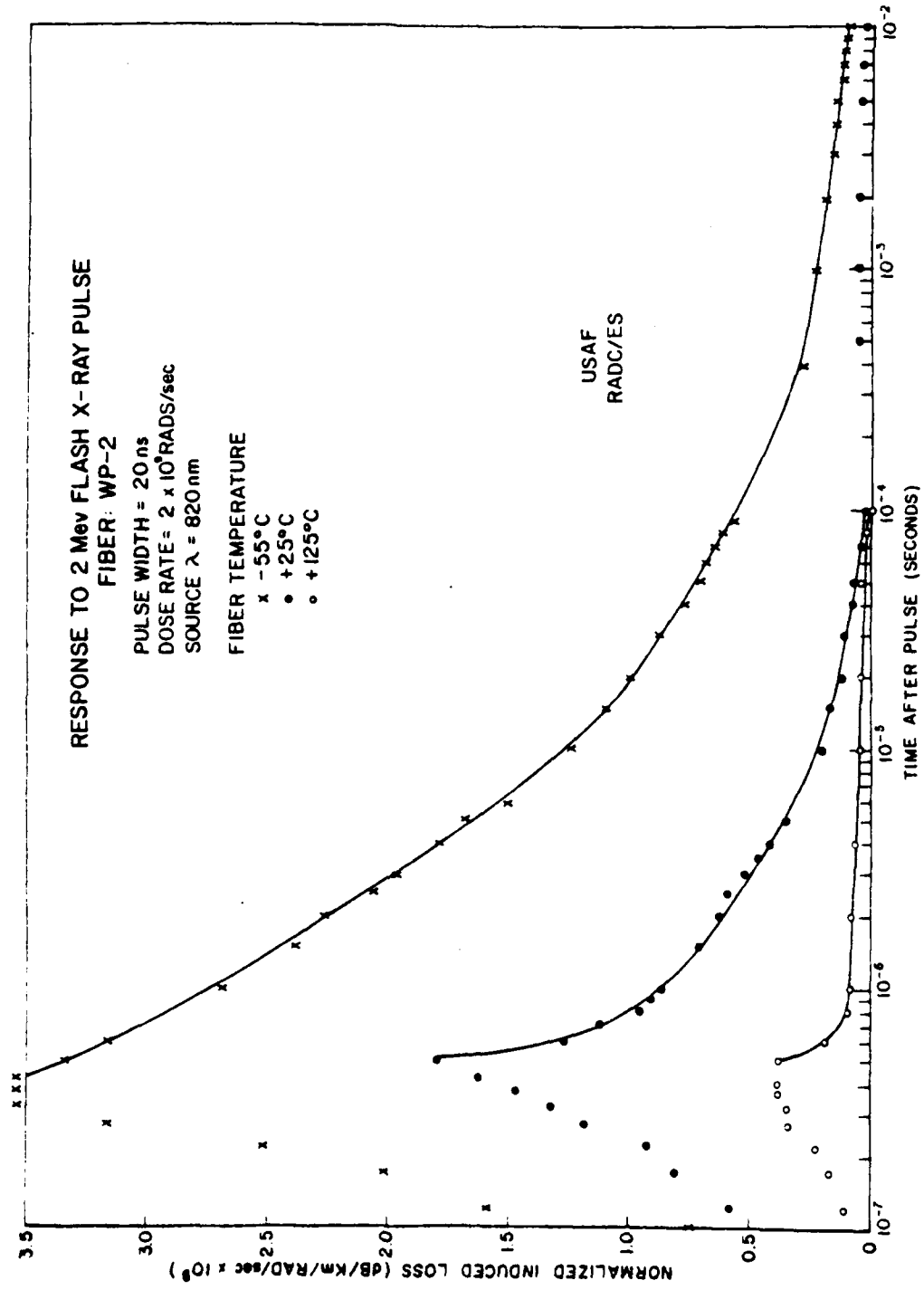


Figure 15  
 -48-

time as the flash x-ray cathode ages. The normalization helps in comparing sets of data by essentially cancelling these variations.

As Figure 15 shows, the amount of transient loss induced in the fiber decreases with increasing temperature, opposite to what was observed in the steady-state irradiations. The rate of decay of the induced loss increases with temperature. The actual induced loss at zero time is undoubtedly much greater than the maximum shown by the data. The initial fluorescent pulse obscures the loss at early times and, since the fluorescence generated in the fiber has a transit time of about 5 nanoseconds per meter of fiber, the true loss is not observable until 400 nanoseconds after the radiation pulse (5 nanoseconds per meter times 80 meters of fiber including leads). At all three temperatures the chart recorder showed a residual loss out to 70 seconds of the order of 0.1 dB/km per  $10^8$  rads per second, which is below the estimated accuracy of the measurement.

For the nominal  $10^8$  rads/sec irradiations (actual dose-rate  $1.6 \times 10^8$  rads/sec) the observed induced losses were close to the limit of measurement. No

induced loss was observable at +125°C. At +25°C the maximum induced loss was approximately 2 dB/km per  $10^8$  rads/sec and at -55°C it was about 4 dB/km per  $10^8$  rads/sec. Loss was detectable beyond the maximum only at -55°C, and this appeared to go to zero at 30  $\mu$ sec after the x-ray burst.

Figure 16 shows the response of fiber WP-6 to a nominal  $10^9$  rads/sec (actual dose rate  $1.1 \times 10^9$  rads/sec) x-ray burst. The results are similar in form to those obtained for WP-2, but the normalized induced losses are about twice those for WP-2 and the rate of recovery is slower.

The  $10^8$  rad/sec (actual dose rate  $1.3 \times 10^8$  rads/sec) exposure showed induced losses near the measurable limit but greater than those for WP-2. At -55°C the maximum observed loss was 8 dB/km per  $10^8$  rads/sec and loss was evident to 7 milliseconds. At +25°C the maximum loss was about 3.5 dB/km per  $10^8$  rads/sec with no loss detectable beyond 5 microseconds. At +125°C a maximum loss of only 1 dB/km per  $10^8$  rads/sec was seen.

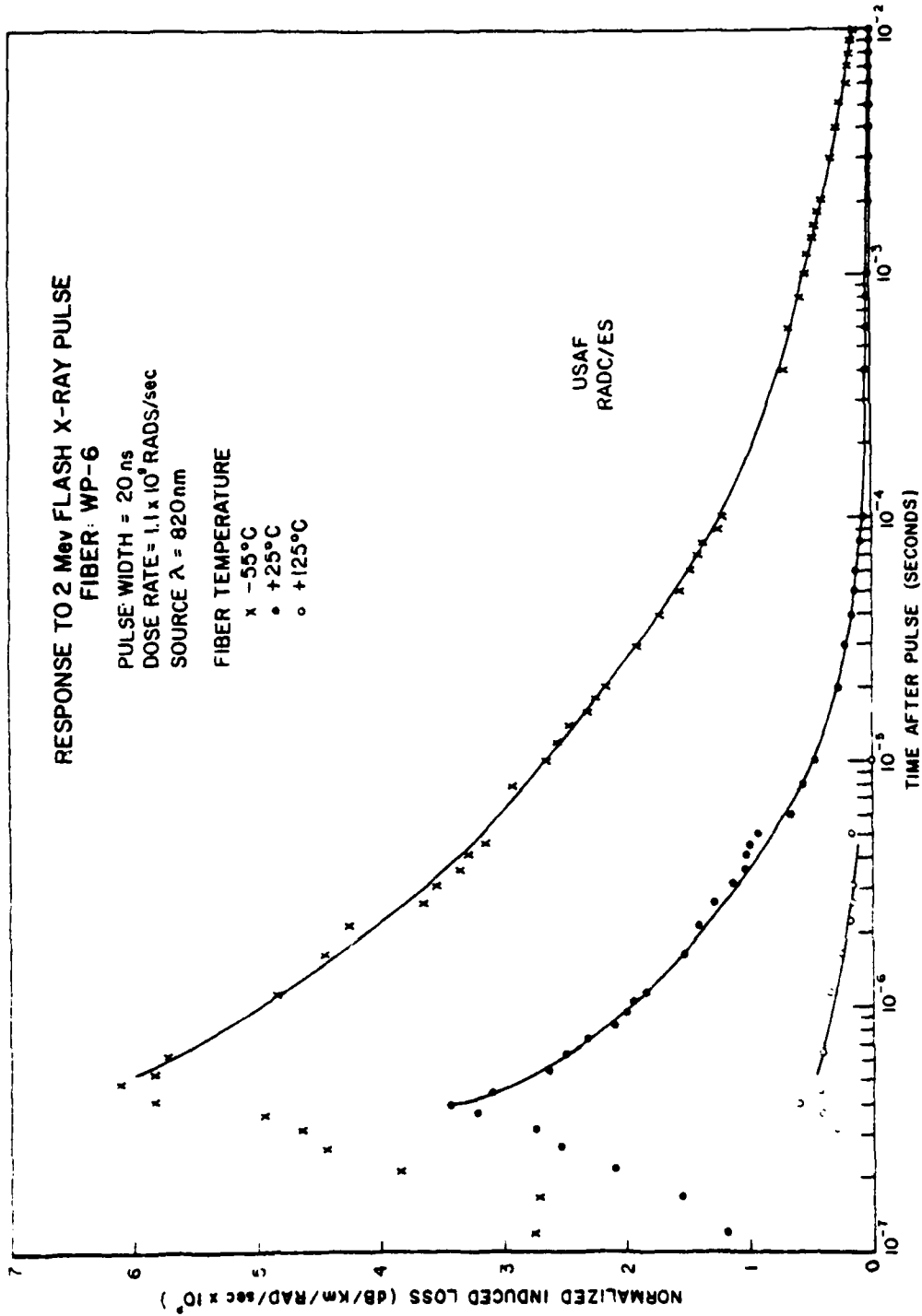


Figure 16

### 3.2 Radiation Effect on Fiber Strength

The strength aspect of the program was not pursued to the extent originally proposed, due to draw problems associated with the laser tower. Perhaps more important, however, was an early decision to concentrate on glass chemistry effects.

Nevertheless, furnace and laser drawn fibers were exposed to  $7.5 \times 10^7$  rads of radiation from the RADC Cobalt 60 source under a bend stress of 75,000 psi (mandrel wrapped). The data given in Table 3 indicate that, although the change upon irradiation was within one standard deviation, a consistent decrease was observed. This amounted to 15% of the mean strength in the furnace drawn fiber and 11% in the laser fiber. The smaller decrease in the laser drawn fiber could result from irradiation of the much narrow flaw distribution expected in this fiber. Corroboration of these results and evaluation of neutron irradiation using better statistics will be attempted when the laser draw system renovation is completed. No conclusions can be drawn at this time.

### 3.3 Effect of Drawing Conditions on Radiation Response

Several experiments were conducted to determine any effect of drawing conditions on the radiation response of the fiber. These tests compared furnace and laser drawn fibers from the same preform. In the case of the furnace, the preform is heated through blackbody radiation and absorption at  $\approx 2000^{\circ}\text{C}$ , and results in a long, gradually tapered draw zone geometry. CO<sub>2</sub> laser heating, on the other hand, produces an intense and confined hot zone through surface

TABLE 3  
MANDREL STRENGTH SUMMARY

<u>FURNACE</u>		<u>CONTROL FIBER</u>	<u>IRRADIATED FIBER</u>
# Samples <sup>2</sup>		19	23
Mean	(MPa) (Kpsi)	1464 212.3	1246 180.7
D. Dev.	(MPa) (Kpsi)	516 74.8	538 78.0
High	(MPa) (Kpsi)	2477 359.2	2566 372.1
Low	(MPa) (Kpsi)	599 86.9	508 73.7
# Fractures Prior to Testing		1	1

<u>LASER</u>			
# Samples <sup>2</sup>		14	18
Mean	(MPa) (Kpsi)	4409 639.4	3921 568.6
S. Dev.	(MPa) (Kpsi)	823 119.3	981 142.3
High	(MPa) (Kpsi)	5720 826.8	5685 824.2
Low	(MPa) (Kpsi)	2948 425.7	2150 311.7
# Fractures Prior to Testing		0	0

- 1) Bend Stress = 75,000 psi
- 2) Test Conditions - Gage Length = 1 meter  
Strain Rate = .10% sec

absorption and the development of an incandescent skin on the preform. This results in a much shorter and more abrupt neck-down geometry.

The experiments were expected to indicate whether the difference in draw-down geometry would induce any radiation sensitive structural defects. Four of the five preforms listed in Table 1 were drawn with both laser and furnace heat sources. The radiation response is given in Table 4. Within experimental error, no differences were observed.

The laser draw facility has been incapable of routinely producing fiber which is comparable in attenuation to furnace drawn fiber. Large periodic and random diameter variations, occurring over relatively short lengths of fiber, are seen as the principle cause of the observed excess attenuation. These result from poor output geometry, temperature variation in cavity cooling water, thermal fluctuations caused by the Rotating Lens System (RLS) and speed variation in the pinch wheels and the preform downfeed mechanism.

The output mode purity of the laser and total power variation has been improved by replacing one damaged mirror, filtering the cavity gases to prevent further damage to the optics, lowering the cavity pressure, and installing a refrigeration unit to provide cooling water. The effect of these changes has been a reduction in output power variation from 25% to less than 2%.

TABLE 4

RADIATION RESPONSE OF FURNACE AND LASER  
DRAWN GERMANIUM BOROSILICATE FIBERS

Induced Attenuation (db/km/krad)	
Furnace	Laser
2.24	1.79
2.36 (2.35)*	2.36
3.26	4.73
2.72	2.40

\*Remeasured fiber from the same preform.

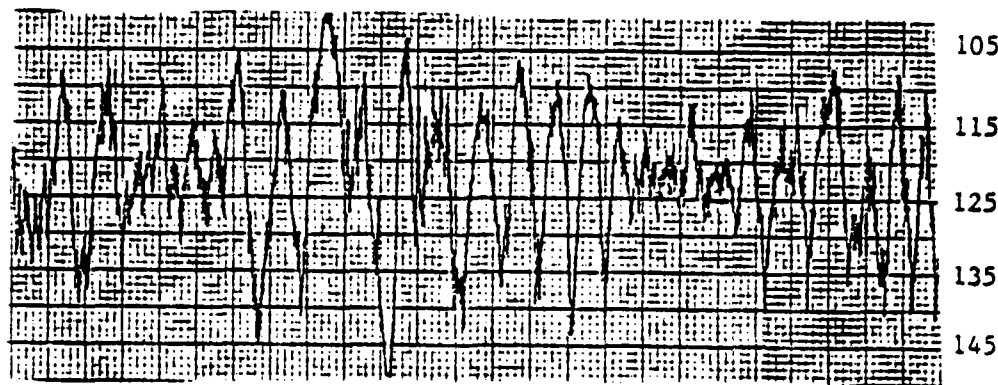
Misalignment of the feed mechanism (preform axis) with respect to the beam delivery optics continued to be a problem causing some out-of-roundness in the fiber. This was corrected by stripping the preform from any contact with the downfeed portion of the tower and guiding it into the back of the faceted reflector with an iris centered on the beam axis.

Figure 17 compares fiber diameter control before (a) and after (b) some attempt was made to address all of the above problem areas. It shows laser fiber drawn at 25 cm/sec and sampled at 200 msec having diameter variation of  $\pm 3\%$  and good circularity (c). The excess attenuation, however, was still 13 db/km higher than furnace drawn material (compared to 20-25 db/km previously). The only apparent explanations for this are an occasional 6-7% peak-to-peak diameter excursion occurring over approximately 2 meter lengths along the fiber and a high frequency periodicity induced by the rotating lens.

Experiments were undertaken to correlate rotating lens speed with the attenuation of the drawn fiber. The same preform was drawn using four different lens speeds while all other drawing parameters were kept constant. Figure 18 shows the results of these experiments. As the rotating lens speed increases, the loss decreases, however, it appears to be leveling off at the highest speeds with approximately 15 - 20 db/km excess loss, presumably due to relatively high random variations. The spatial wavelengths

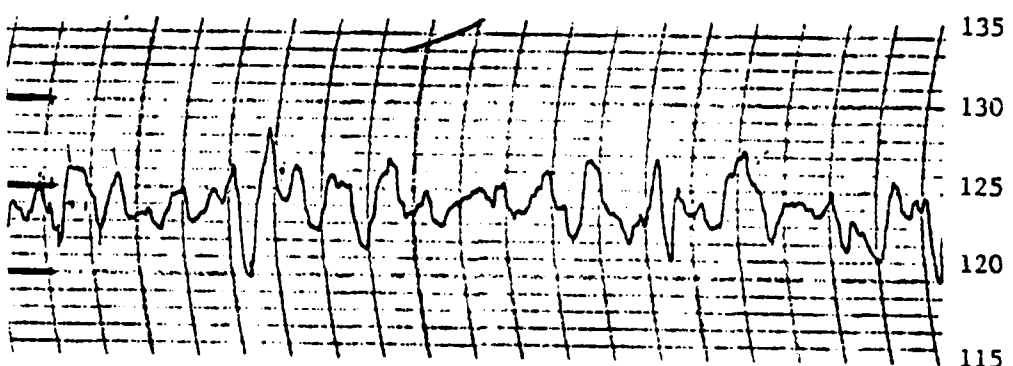
RADC-12

(a)



RADC-56

(b)



RADC-56

(c)

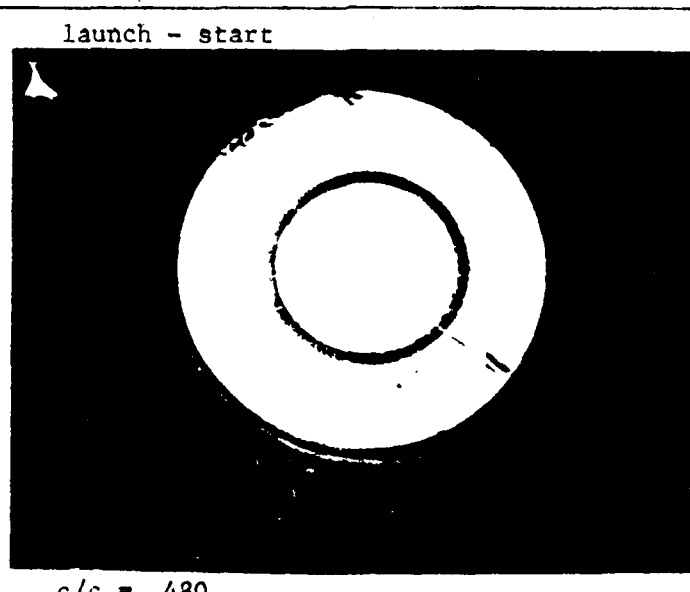


Figure 17

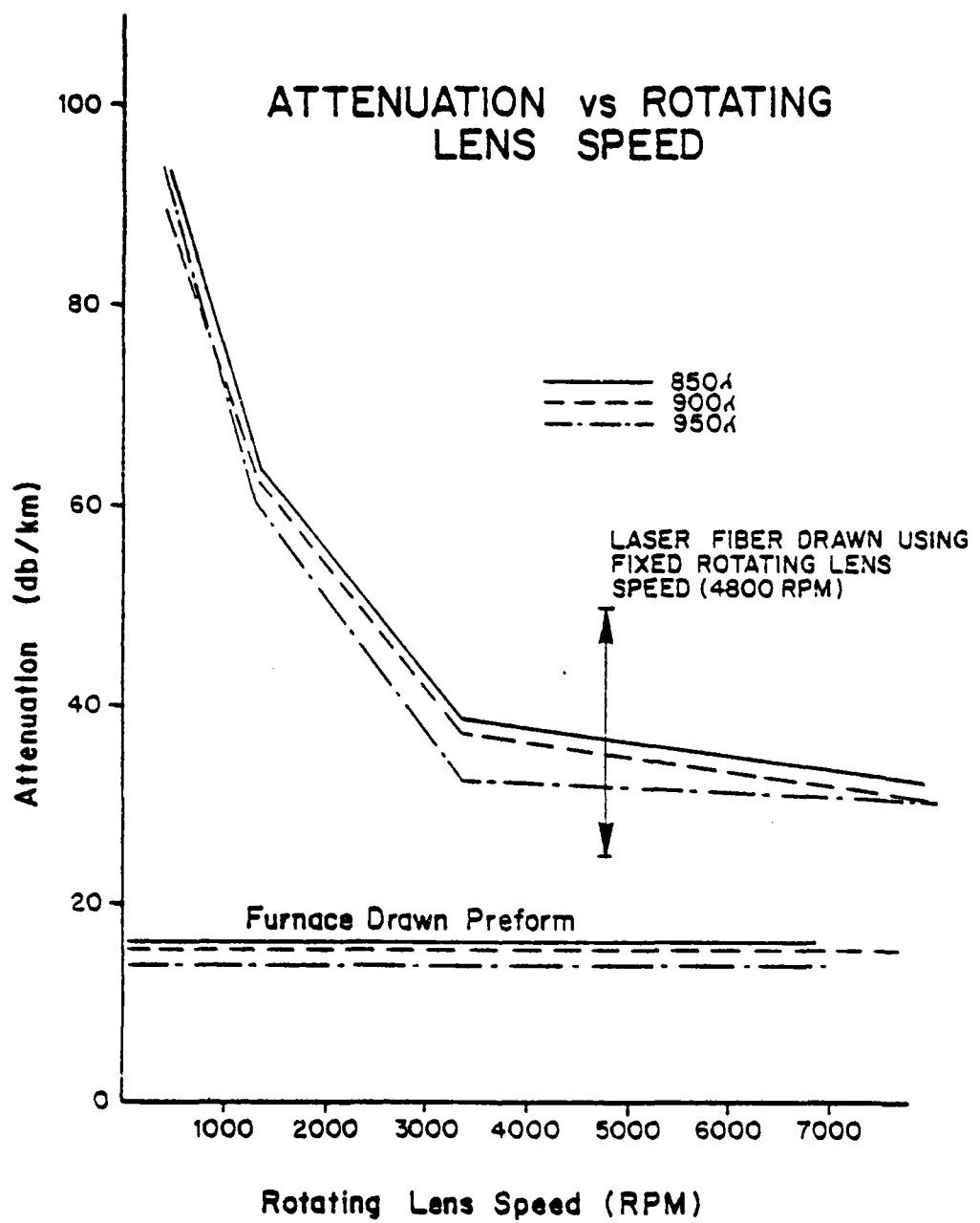
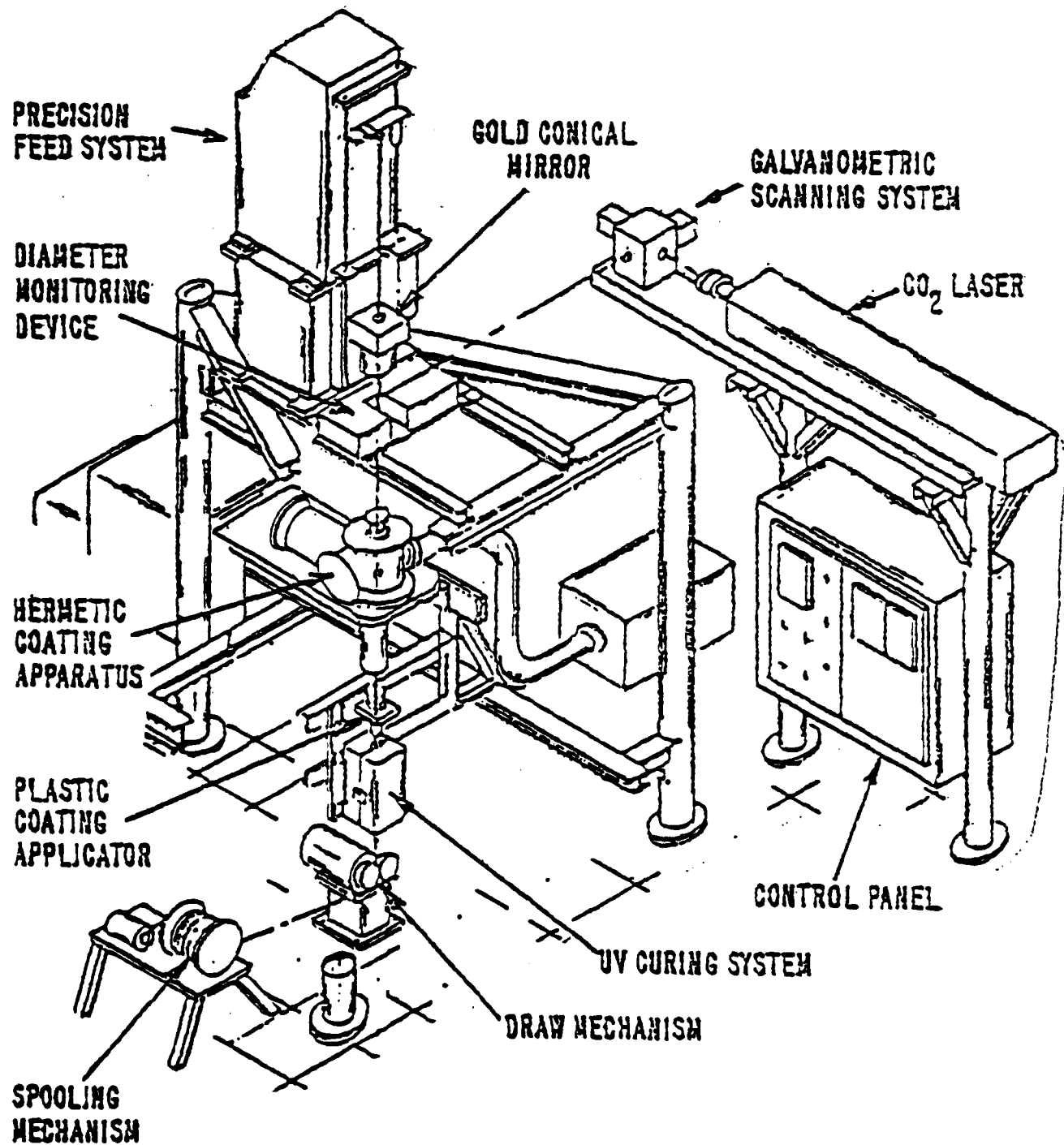


Figure 18

of the rotating lens induced diameter variations are in the range of 2 to 15 mm, and are believed to be responsible for converting propagating modes to radiative cladding modes.

Since a finite small hot zone is generated by the RLS, better diameter control can be obtained with smaller preforms as a result of a longer and more stable neck geometry. The ability to increase the spatial wavelength of the periodic variation and decrease its amplitude by using faster draw speeds is another benefit of this approach. Combining these techniques enabled us to produce a laser drawn fiber whose pre-irradiation physical and optical properties were comparable to those of furnace drawn fiber (RADC #71-L).

These results, however, were not reproducible on a routine basis. In addition, re-examination of the optical delivery system indicated that the rotating lens was severely distorting the output beam. In order to correct these problems, a new laser draw tower was built that will be operational in the next contract period. This tower, shown schematically in Figure 19, will have a precision feed and draw system that are interlocked to a diameter monitoring device which will aid in diameter control. A galvanometric scanning system (GSS) will replace the present rotating lens. Some advantages of the GSS are that it operates at higher frequencies, neck-down geometry is better controlled, and there is less silica vaporization from the preform surface (11).



Laser Draw Tower

The tower is designed to accommodate an hermetic coating apparatus used for experiments on in-line plasma deposition of metallic and dielectric coatings. Figure 9 shows the position of the hermetic coating deposition apparatus relative to the various other components. The tower design allows the coating apparatus to be easily removed for other drawing experiments using waveguide and synthetic silica preforms. We expect that this new facility will greatly improve the performance of laser drawn fiber.

#### 4.0 DISCUSSION AND CONCLUSIONS

##### 4.1 Compositional and Draw Effects

The data presented in Section 3.1.1 and 3.1.2, on the steady-state and transient response of boron, phosphorous and hydroxyl doped germanium silicate fibers, are consistent with published results<sup>(1,2)</sup>, when wavelength and dose rate effects are considered. The behavior of fibers containing cerium and antimony indicate that multivalent dopants can be used to modify favorably the radiation response of optical fibers, without adversely affecting their optical properties, by tailoring fiber compositions to meet specific requirements.

The substitution of phosphorous for boron in germanium-borosilicate fibers significantly reduced the induced loss under transient radiation conditions, but increased the rate of induced loss by an order of magnitude under steady-state irradiation. However, the addition of antimony to the phosphorous-doped fiber, improved the steady-state radiation response with no measureable effect on its transient response, other than increased fluorescence at very short times. This fiber, therefore, offers an improved possibility of meeting requirements under both radiation conditions.

The nonlinear response of the fiber doped with cerium and boron suggests the possibility that the presence of cerium produces a significant change in the electron-hole trapping processes responsible for radiation induced loss. The decrease in rate of induced loss with increasing dose is not the result of annealing during irradiation. As described in Section 2, the dose rate was increased in steps from 1 to 16 rads/sec during the

irradiation. If significant simultaneous annealing was occurring, one would expect an increase in rate of induced loss with increasing dose rate. A more likely explanation of the high initial slope, is linked to a suspected malfunction of the linac during the irradiation. Subsequently identified instabilities, resulting in large variations in dose per pulse, are the probable cause of the non-linear behavior. Further measurements on different cerium concentration in various base glasses using both linac and cobalt-60 sources, are needed before the value of cerium as a radiation hardening dopant can be established. The present results indicate, however, that cerium doped fiber has potential for improved radiation hardness.

There appears to be no difference in the radiation response between germanium borosilicate fibers drawn from the same preform using resistance furnace or laser heat sources.

#### 4.2 Temperature Effects

Under steady-state irradiation, both fibers tested showed an increase in the induced loss per unit dose with increasing temperature. For a quantitative comparison of this effect, Table 5 gives the initial slopes for the data plotted in Figures 10, 12 and 13. The data in Table 5 also show the significantly lower rates of induced loss for the fiber (WP-6), having slightly higher numerical aperture, and the good correlation between linac and cobalt-60 results. The initial slope of the first length of fiber WP-6 irradiated at +125°C with linac x-rays is very close to the cobalt-60 result.

TABLE 5

INITIAL INDUCED LOSS PER UNIT DOSE FOR  
STEADY-STATE IRRADIATIONS (dB/km - krad)

T(°C)	LINAC X-RAYS		
	WP-2	WP-6	WP-6
-55	19	12	12
+25	23	17	16
+125	31	16, 21*	23

\*Full data not shown because of low linac output.

The data on the annealing of induced loss following steady-state irradiation, shown in Figures 11 and 14, can be described by the relationship

$$\frac{L}{L_0} = A_1 e^{-t/\tau_1} + A_2 e^{-t/\tau_2} + A_3 e^{-t/\tau_3}$$

where  $L_0$  = induced loss at end of irradiation  
 $L$  = loss at time  $t$  (minutes)  
 $A_1, A_2, A_3, \tau_1, \tau_2, \tau_3$  = constants

A least squares fit of the data to this expression yielded the constants shown in Table 6.

Considering the  $\tau$ 's as time constants,  $\tau_1$  dominates the long-term recovery of induced loss. It is essentially unchanged for the temperature change from  $-55^{\circ}\text{C}$  to  $+25^{\circ}\text{C}$ , but decreases an order of magnitude at  $+125^{\circ}\text{C}$ . The similar temperature dependence of the constants  $A_1, A_2$  and  $A_3$  may be related to the observation that when the temperature of the fiber irradiated at  $-55^{\circ}\text{C}$ , was subsequently raised to  $+25^{\circ}\text{C}$ , the loss was 1.2 times that at the end of irradiation, and essentially identical to that observed when the fibers were irradiated at  $+25^{\circ}\text{C}$ .

The results of the transient radiation induced loss measurements can also be expressed in closed form. In this case the best fits were obtained with the expression:

$$\frac{L}{D} = \frac{a}{1+bt^n}$$

TABLE 6  
CONSTANTS FOR ANNEALING OF INDUCED LOSS

FIBER	T(°C)	A <sub>1</sub>	τ <sub>1</sub>	A <sub>2</sub>	τ <sub>2</sub>	A <sub>3</sub>	A <sub>3</sub>
WP-2	-55	1	$2.1 \times 10^4$	0	---	0	---
	+25	0.968	$2.4 \times 10^4$	0.020	$2 \times 10^2$	0.012	38.7
	+125	0.664	$1.8 \times 10^3$	0.193	$2.4 \times 10^2$	0.143	43.8
WP-6	-55	0.952	$2.8 \times 10^4$	0.031	80.8	0.017	5.62
	+25	0.96	$3 \times 10^4$	0.030	$1.4 \times 10^2$	0.010	10.3
	+125	0.696	$2.9 \times 10^3$	0.211	$1.7 \times 10^2$	0.093	31.2

where  $L$  = loss at time  $t$  (in microseconds) (2)  
 $D$  = dose rate in units of  $10^8$  rads per second  
 $a, b, n$  = constants

Table 7 lists the constants for equation (2) derived from the data. No entries appear in Table 7 for fiber WP-2 at  $+125^{\circ}\text{C}$  because the data obtained was inadequate to obtain a reasonable fit. The constants listed for equation (2) give a good fit to the data to at least 1 millisecond for the  $-55^{\circ}\text{C}$ , results, and to at least 50 microseconds for the  $+25^{\circ}\text{C}$  results. Although the fit at  $+125^{\circ}\text{C}$  had a correlation coefficient greater than 0.9, most of the data is close to the estimated limit of accuracy of the measurements. The negative values obtained for the constants "a" and "b" are probably the result of timing errors in the data. In both cases, with the constants derived, equation (2) goes to infinity at approximately 20 nanoseconds, which implies that the timing errors are of that order.

Ignoring the negative signs, the constant "a" is a measure of the induced loss at zero time (assuming fits can be extrapolated at this point). It is interesting that "a" is not strongly temperature dependent between  $-55^{\circ}\text{C}$  and  $+25^{\circ}\text{C}$ , but changes significantly from  $+25^{\circ}\text{C}$  to  $+125^{\circ}\text{C}$ , similar to the behavior of  $\tau_1$  in equation (1) for recovery following steady-state irradiation. The constants "b" and "n" are indicators of the rate of recovery of induced loss following the x-ray pulse and show that recovery is much more rapid at  $+25^{\circ}\text{C}$  than at  $-55^{\circ}\text{C}$ . No valid comments can be made on the values of "b" and "n" at  $+125^{\circ}\text{C}$  because of the limited accuracy of the original data.

TABLE 7

CONTANTS FOR THE RECOVERY OF INDUCED LOSS FOLLOWING  
FLASH X-RAY PULSE

FIBER	T( $^{\circ}$ C)	a	b	n
WP-2	-55	9.68	2.58	0.400
	+25	-8.34	-9.62	0.601
WP-6	-55	12.7	1.53	0.392
	+25	17.1	6.49	0.731
	+125	-0.94	-3.92	0.34

Although measurements of the temperature dependence of radiation response of optical fibers reported here were performed with specific applications in mind, the data gives some clues to the physical processes involved in radiation induced loss. The increase in rate of induced loss with increasing temperature observed in the steady-state irradiations implies that the electrons and/or holes released during irradiation are eventually retained in deeper trapping levels at lower temperatures than at higher temperatures. At the deeper levels the optical absorption band of the trapped species would be at shorter wavelengths and have less effect in the 800nm region where the measurements were made. As the temperature increases, equilibrium trapping occurs at more shallow levels, causing a shift in absorption to longer wavelengths and an increase in loss at the wavelength of the measurements. The continuous increase in loss following irradiation at -55°C and return to +125°C also supports this model, which implies a distribution of trapping levels that can be treated as continuous. Similar models have been successfully applied to the description of electrical conduction phenomena in  $\text{SiO}_2$ .<sup>(12)</sup>

For the transient radiation response, the initial density of electron-hole pairs generated, and therefore the initial induced loss, for any given dose and dose-rate should be independent of temperature.<sup>(13)</sup> The low value of the constant "a" (Table 7 and equation 2) derived at +125°C is undoubtedly the result of either insufficient data or the limited accuracy attainable at that temperature.

Finally it should be noted that the temperature results reported here are for specific fiber types. Although the composition and processing techniques are not unique, the data should not be generalized as representative of all germanium phosphosilicate optical fibers.

#### 5.0 INTERACTIVE PROGRAM

An important aspect of this contract was frequent technical interaction between RADC and Galileo personnel. In the early months of the program the emphasis was on establishing a high temperature draw capability at RADC/HAFB. Galileo contributed to the design and construction of this facility of providing engineering prints, coating applicators, a draw mechanism, and consultation on the selection of purchased components.

In addition, numerous technical exchange visits occurred for the purpose of experiment planning and review. These periodic meetings took place at a frequency greater than one per month.

#### REFERENCES

1. S. Share, R.M. McCracken and I. Aggarwal, IEEE Trans. on Nuclear Science, NS-25, 1288 (1978).
2. E.J. Friebele, P.C. Schultz, M.E. Gingerrich and L.M. Hayden, Proceedings of the Conference on Optical Fiber Communication, March, 1979.
3. H. Posen, J.A. Wall and R.E. Jaeger, Proceedings of the Conference on the Physics of Fiber Optics, 27-50-80, May, 1980.
4. S. Share and J. Wasilik, IEEE Trans. on Nuclear Science, NS-26, 4802, (1979).
5. H. Posen, J.A. Wall and R.E. Jaeger, Proceedings of the Conference on the Physics of Fiber Optics, 28-50-80, May, 1980.
6. G.S. Monk, Nucleonics, 10, No. 11, 55 (1952).
7. A. Bishay, J. Non-Crystalline Solids, 3, 54 (1970).
8. Personal Communication of Data Prior to Publication, (Reference 1).
9. Personal Communication of Data Prior to Publication, (E.J. Friebele, M.E. Gingerich and G.W. Sigel Jr., Applied Physics Letters, 32 (10), 619 (1978)).
10. Reference for Cerenkov effect.
11. R.C. Oehrle, Applied Optics, 18 (4), Feb. (1979).
12. O.L. Curtis and J.R. Srour, J. Appl. Phys. 48, 3819, (1977).
13. P.L. Mattern, L.M. Watkins, C.D. Skoog and E.H. Barsis, IEEE Trans. on Nuclear Science, NS-22, 2468 (1975).

APPENDIX A

- "The Role of the Multidopants Sb/P in Radiation Hardening of Optical Fibers"  
By: R. Jaeger, J.A. Wall, H. Posen
- "Radiation Performance of Germanium Phosphosilicate Optical Fibers as a Function of Temperature"  
By: R. Jaeger, J.A. Wall, H. Posen

The Role of the Multidopants Sb/P in Radiation Hardening of  
Optical Fibers

J. A. Wall, H. Posen\*, Deputy for Electronic Technology,  
Rome Air Development Center, Solid State Sciences Division, Hanscom AFB, MA  
01731 (617)861-4031

R. Jaeger, Galileo Electro-Optics Co.,  
Galileo Park, Sturbridge, MA 01518

Introduction

It is well known that small changes in the composition and impurity content of glasses can significantly affect their responses to energetic radiation, yet there have been very few studies of radiation effects on optical fibers in which these factors were known and controlled.<sup>1</sup> RADC has initiated a program to study the effects of radiation on optical fibers fabricated under well documented conditions from preform to drawing process. This paper presents preliminary results obtained as part of that program on the radiation response of germanium-silicate fibers doped with phosphorous and/or antimony.

Experimental

Several step index fiber preforms with  $GeO_2$ - $B_2O_3$ - $SiO_2$  cores and T0-8 cladding were prepared using the CVD process. The nominal vapor composition of the cores before deposition was, in mole percent, 48%  $SiO_2$ , 50%  $GeO_2$ , and 2%  $B_2O_3$ . Modifications were made in some of the core compositions, including the deliberate introduction of OH. Fibers drawn from these preforms were tested for their real-time response to steady state radiation and the results used to establish a baseline for the study of dopant effects. Additional preforms were then fabricated with compounds of phosphorous and/or antimony added to the vapor stream in place of, or in addition to, the boron. Table 1 lists the composition and optical properties of the four fibers on which radiation test results will be reported.

Table 1  
Fiber Compositions and Optical Properties

Mole % in Gas Stream					OH ppm	N.A.	Attenuation at 900nm dB/km
Si	Ge	B	P	Sb			
61.4	37.2	1.4	-	--	8	0.17	8.3
65.9	33.9	-	0.2	--	3	0.19	7.9
61.3	36.5	1.4	-	0.8	13	0.18	6.8
61.7	37.4	-	0.2	0.8	2	0.21	5.3

\*Deceased, December 1979

The radiation responses of the fibers were measured under both steady-state and transient conditions. The steady-state irradiations were performed using x-rays produced by 10 MeV electrons from the RADC linear accelerator (linac) incident on a tungsten target. The linac was set to produce 4.5usec wide pulses of electrons and the pulse rate could be varied at will. This made it possible to change the average dose-rate to the fibers instantaneously during, and without interrupting, the irradiation to test dose-rate effects. 25 meters of fiber were wound on 13 cm diameter, 1 cm thick reels and positioned relative to the x-ray target to receive approximately one rad per linac pulse. The light source was a 905 nm LED pulsed with 10usec wide pulses at a rate of 100 kilohertz. The detector was an APD-amplifier module. The source and detector were located out of the direct x-ray beam and were shielded from scattered radiation by lead bricks. The output of the detector was connected to an oscilloscope in the experiment control area which was used to observe and photograph the amplitude of the light pulses transmitted by the fiber during the irradiation. The fibers were irradiated until the transmitted pulse amplitude dropped to half its pre-irradiation value. At the beginning of the irradiations the linac pulse rate was set for 1 pps. The pulse rate was doubled at intervals during the irradiation. The maximum rate reached during any of the irradiations was 16 pps, giving an average dose-rate range of approximately 1-16 rads/sec.

Dosimetry for the steady-state irradiations was performed using thermoluminescent dosimeters (TLD's) placed in quadature around the reels on both sides of the reels and in line with the fiber position. The TLD's measured the total dose accumulated by the fiber. During the irradiation, the number of linac pulses accumulated was registered on a counter and the fiber transmission was measured as a function of the number of linac pulses. Following the irradiation the total dose to the fiber as measured by the TLD's was divided by the total number of linac pulses accumulated to obtain an accurate measure of dose per linac pulse. The data was then converted to fiber transmission as a function of dose.

The transient radiation response measurements were performed using the RADC flash x-ray generator which produces single 20 nanosecond wide x-ray pulses of nominal 2 MeV peak energy. The APD module, which had a D.C. to 40 megahertz bandwidth, used for the steady-state irradiations was also used as the detector for these measurements. The LED light source was replaced by a quartz iodide lamp and monochromator set at 905 nm. The fiber lengths (25 meters) and reels were the same as for the steady-state tests. The light source was located in the irradiation area but out of the x-ray beam path. The output end of the fiber being irradiated was coupled to the detector in the experiment control area through a fiber-optic link. The output of the detector was connected to four oscilloscope inputs to obtain measurements over a time span from less than 50 nanoseconds to 100 milliseconds. The dose-rate received by the fiber was measured by means of a small PIN diode in contact with the fiber on the reel.

### Results

Except for small deviations (which could have been instrumental in origin) below about 2 kilorads, all of the fibers tested showed a very linear induced loss as a function of dose over the range of doses used in the steady-state irradiations.

No changes in this linearity were observed as the dose-rates were changed. For the nine "baseline" germanium-borosilicate fibers, the average rate of induced loss was 2.9 dB/km per kilorad with a standard deviation of 1.0 dB/km per kilorad. Five of these nine had the same mole percentages of silicon, germanium and boron in the vapor stream and they showed an average rate of induced loss of  $2.3 \pm 0.4$  dB/km per kilorad.

Figure 1 shows the results of the steady-state irradiations of the doped fibers and one of the baseline fibers. The addition of antimony to the vapor stream increased the rate of induced loss by approximately a factor of 4 over that of the baseline fiber, and substitution of phosphorous for boron increased the rate of induced loss by about a factor of 10. The addition of antimony to a phosphorous-doped fiber reduced the rate of induced loss to nearly the same as that for the antimony-boron combination.

In the transient tests the fibers were exposed to nominal dose rates of  $10^8$  and  $10^9$  rads/sec. At both dose rates an initial fluorescent pulse of sufficient amplitude to overload the detector module was observed for all fibers. The detector overload appeared as broadening of the pulse for up to 200 nanoseconds at the  $10^8$  rad/sec level and up to 600 nanoseconds at the  $10^9$  rad/sec level. This prevented loss measurements at times shorter than these. At  $10^8$  rads/sec only the boron and antimony + boron doped fibers showed induced losses and these losses were too small to make meaningful measurements from the oscilloscope photographs. Figure 2 shows the induced losses, at the nominal  $10^9$  rads/sec level (actual dose-rate  $1.7 \times 10^9$  rads/sec) as a function of time over part of the time-span covered by the measurements. The actual measured losses have been divided by dose-rate in units of  $10^8$  rads/sec in figure 2 (normalized induced loss) for better comparison of results obtained for the different fibers. This is necessary because the output of the flash x-ray generator can vary by about 10% from pulse to pulse. No induced loss was observed for either fiber doped with phosphorous.

The antimony and boron doped fiber appears to show less induced loss than the boron doped fiber. However, there was an indication of a long (at least one microsecond) duration fluorescence generated in that fiber which could cause the measured loss to be less than the actual induced loss. The generation of this fluorescence was confirmed by tests of two other fibers doped with 2.5% and 4% antimony. For these fibers the fluorescence was evident for 200 and 600 microseconds, respectively, with no light input to the fibers.

For all the fibers tested under transient radiation the induced losses became undetectable within 100 milliseconds.

### Conclusions

The substitution of phosphorous for boron in germanium-borosilicate fibers significantly reduced the induced loss under transient radiation conditions but increased the rate of induced loss by an order of magnitude under steady-state irradiation. The addition of antimony to the phosphorous-doped fiber improved the steady-state radiation response with no measurable effect on its transient response.

At present, the attainment of minimal induced loss under transient radiation appears incompatible with optimum fiber response under steady-state irradiation. The germanium-phosphosilicate fiber doped with antimony offers an improved possibility of meeting requirements under both radiation conditions. This result suggests that further improvements in the radiation hardness of optical fibers could result from continued, controlled investigations of the relationship between fiber composition and radiation response.

#### REFERENCES

1. S. Share, R. M. McCracken and I. Aggarwal, IEEE Trans. on Nuclear Science, NS-25, 1288 (1978).

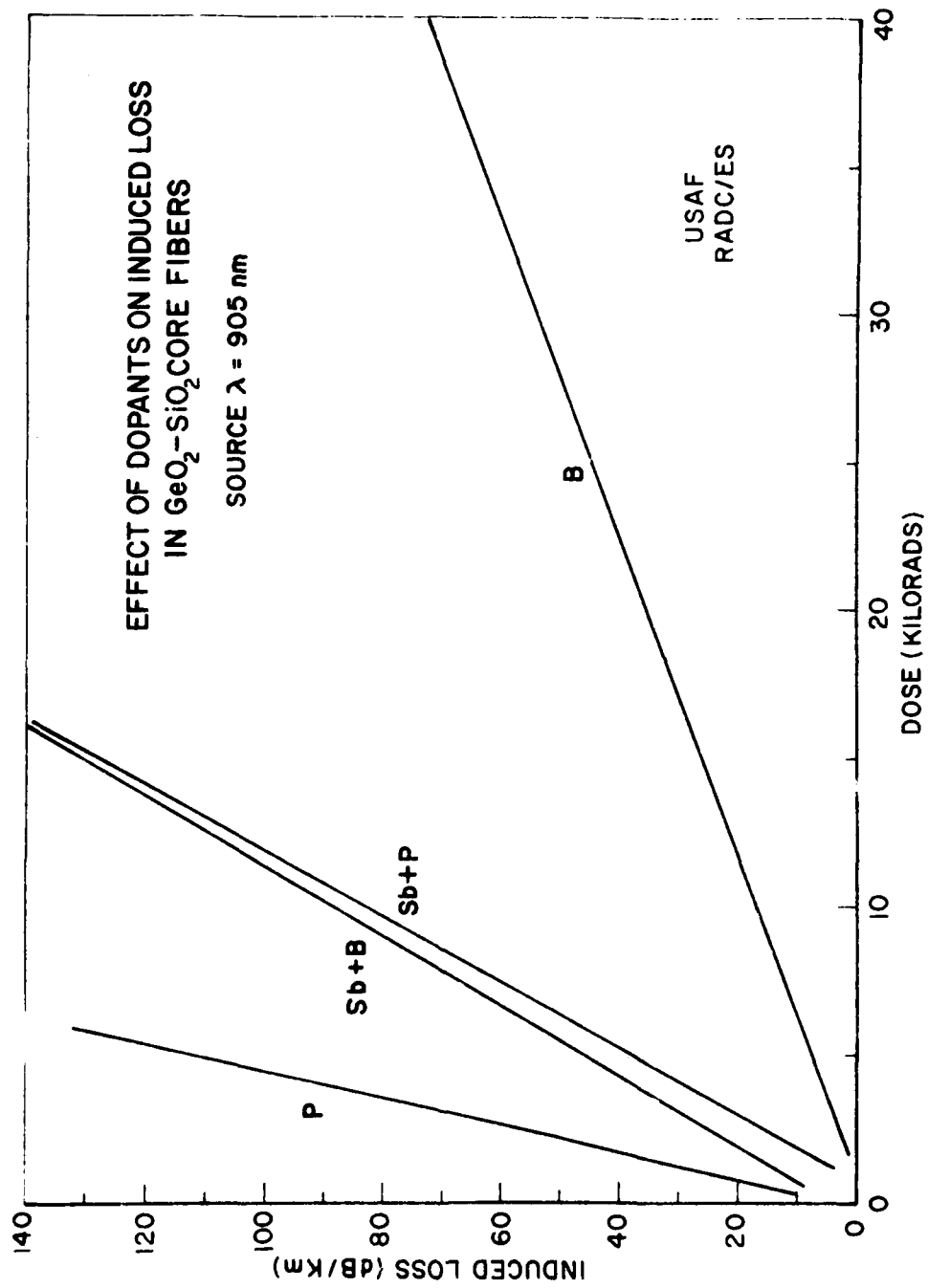


Figure 1

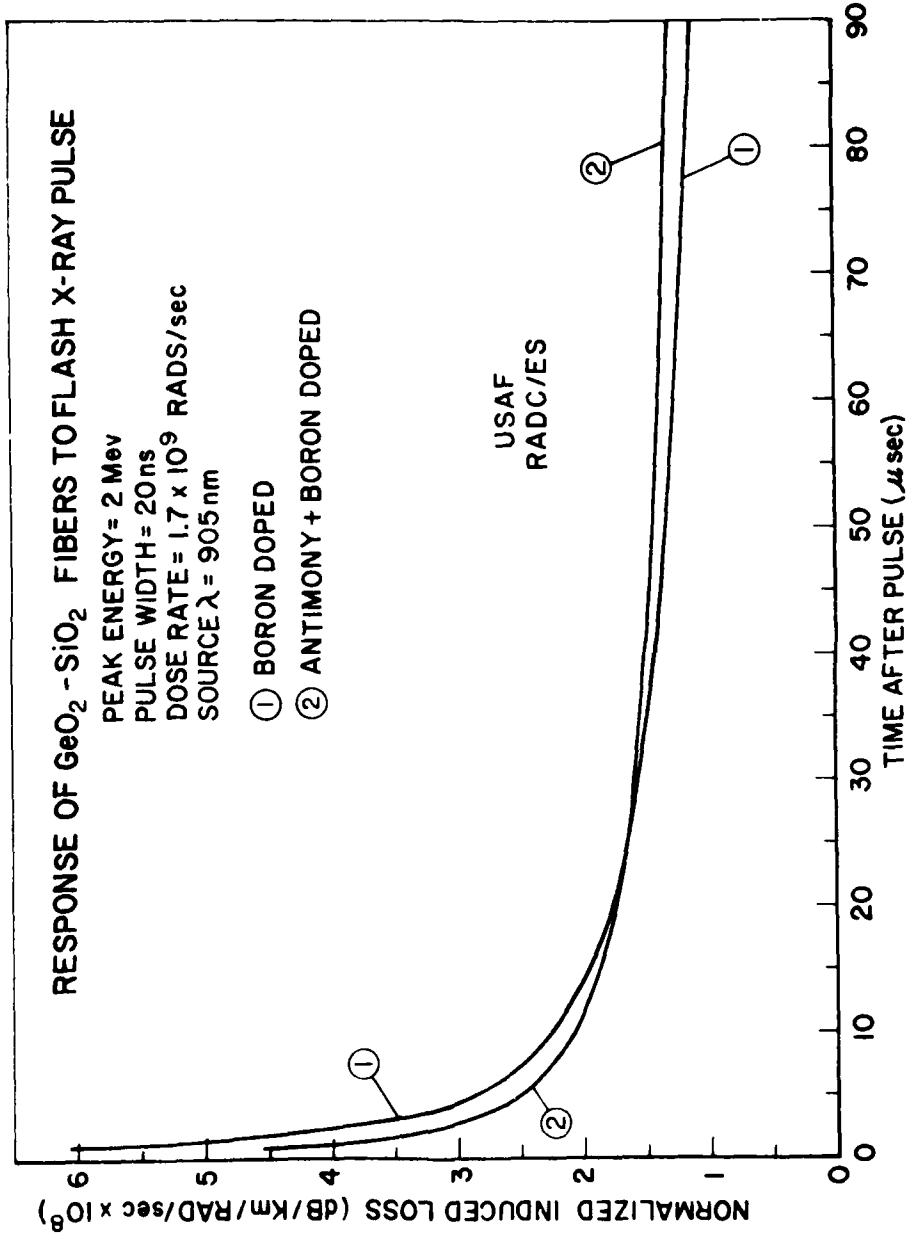


Figure 2

## Radiation Performance of Germanium Phosphosilicate Optical Fibers as a Function of Temperature

J. A. Wall, H. Posen\*, Deputy for Electronic Technology  
Rome Air Development Center, Solid State Sciences Division, Hanscom AFB, MA  
01731, (617)861-4031

R. Jaeger, Galileo Electro Optics Co.,  
Galileo Park, Sturbridge, MA 01518

### Introduction

In the application of optical fibers to military systems, one of the principle types of fiber being considered by designers is the so-called "fat" fiber with high numerical aperture. The reasons for this choice are high source coupling efficiency and ease of handling in the field. Also, fibers with phosphorous-doped cores are considered desirable because of their known superior recovery characteristics in transient radiation environments. However, no real-time radiation response tests of this type of fiber over the mil-spec temperature range of -55°C to +125°C have previously been performed. This paper presents data on such tests.

The tests were performed in response to a request from the Air Force Avionics Laboratory for information on a commercially available Germanium Phosphosilicate fiber. The fiber has a core/clad ratio of 125/200 $\mu$ m and a numerical aperture of 0.25. Unjacketed versions of this fiber were specially fabricated for these tests. Real-time steady-state and transient radiation response tests were performed at temperatures of -55°C, +25°C and +125°C on two of these fibers. For reference purposes, the fibers are designated WP-2 and WP-6, with WP-6 having a higher germanium content in the core and a numerical aperture of 0.26. All tests were performed on lengths of fiber taken from a single draw in order to avoid any variations in test results that might be caused by differences between preforms or drawing processes.

### Experimental Procedures

A temperature control chamber, specially designed for use with the RADC/ES radiation facilities, was constructed for the tests. Except for heating elements and wiring which are located some distance from the fiber position, it is made of all low atomic number materials to prevent perturbation of the radiation fields at the sample position. The walls are double plywood with fiberglass insulation and the sample chamber is aluminum. The chamber is divided by aluminum baffles to one of which is mounted a 900 watt heating element used to attain temperatures up to +150°C. The lower part of the chamber serves as a liquid nitrogen reservoir. The fibers are wound on 13 cm diameter, 1.5 cm thick aluminum reels which mount on the upper end of a moveable aluminum strut. The base of the strut rests on the bottom of the chamber so that it serves as a cold finger when the reservoir is filled with liquid nitrogen. A low-power heating element attached to the strut controls the temperature, measured by a thermocouple, at the sample position.

\*Deceased, December 1979

Temperatures are maintained to within within  $\pm 1^{\circ}\text{C}$  by proportional controllers and thyristor packs mounted in a console which can be located up to 25 meters from the chamber and radiation sources. The console also includes a digital thermometer for continuous temperature monitoring and an automatic liquid nitrogen fill controller which, in conjunction with a 60 liter pressurized dewar, can maintain the lower temperatures for at least six hours.

Steady-state irradiations were performed using x-rays generated by 10 MeV electrons incident on a tungsten target. The electron source was the RADC linear accelerator (linac) which was set to produce electron pulses 4.5 $\mu\text{sec}$  wide at an approximate rate of 5 pps. The fiber, mounted in the temperature control chamber, was positioned relative to the x-ray target so that it received a uniform irradiation of about 0.5 rads per (linac) pulse. The ends of the fiber were brought out of the chamber and coupled to an 850 nm LED source operated in continuous mode and a PIN photodiode-amplifier detector. The source and detector were located out of the direct x-ray beam and shielded from scattered radiation by two inches of lead. The output of the detector was fed to the experimental control area by coaxial cable and connected to a digital voltmeter and chart recorder for continuous observation of the fiber transmission. A pulse counter was used to measure the accumulated number of linac pulses. The voltmeter reading was recorded as a function of total linac pulses at frequent intervals while the chart recorder provided a continuous reading of the detector output as a function of time. Following the irradiation, the chart recorder was used to monitor recovery of the induced loss.

Dosimetry was performed using thermo-luminescent dosimeters (TLD's) mounted in quadrature on each side of the fiber reel at the fiber position. The TLD's measured the total dose to which the fiber was exposed during the irradiation. Dividing this total dose by the total number of linac pulses generated during the irradiation gave an accurate measure of the dose produced by each linac pulse. The data taken in terms of induced loss as a function of accumulated linac pulses was then converted to loss as a function of dose.

Because the linac is a pulsed radiation source, a set of irradiations was also performed on one of the fibers using the RADC Co-60 source to check the validity of using the linac for steady-state tests. The arrangement was similar to that using the linac except that the source and detector were located outside the cobalt cell and an ionization chamber was used to monitor accumulated dose. The ionization chamber could not be operated at the temperature extremes in these tests, so it was located outside and adjacent to the temperature control chamber in a position where it received approximately the same exposure as the fiber. The chamber readout was set to indicate accumulated dose and its output connected to a second pen on the chart recorder so that induced loss and accumulated dose could be measured simultaneously. As with the linac irradiations, TLD's were used as a final calibration of the dose indicated by the ionization chamber since it was not located at the fiber position. These irradiations also provided a calibration of the TLD's at  $+125^{\circ}\text{C}$ , a temperature at which they had never before been irradiated.

The transient tests were performed using the RADC flash x-ray generator which produces a 20 nanosecond pulse of nominal 2 MeV peak energy. Tests were performed at two dose-rates on the order of  $10^8$  rads per second and  $10^9$  rads per second. An 820 nm laser diode operated in continuous mode was used as the light source

and a PIN photodiode and 50 megahertz bandwidth amplifier was used as the detector. The source was located in the irradiation area but out of the x-ray beam. The output end of the fiber was coupled through a fiber-optic link to the detector located in the experiment control area. The detector output was connected to four oscilloscope inputs and an X-Y recorder (with time base) to obtain a time span from less than 50 nanoseconds to over 60 seconds. Dosimetry was performed using a small pin diode in direct contact with the fiber on the reel, except at +125°C where the PIN could not be operated. In the latter case, dose-rate was estimated from the average of dose-rates measured in preceding "shots" at lower temperatures in the same position relative to the flash x-ray target.

For both the steady state and transient tests, 75 meter lengths of fiber were irradiated. New lengths of fiber were used for each irradiation with the exception of the transient tests at  $10^8$  rads per second where it was found in preliminary trials that the results of several "shots" on the same fiber were indistinguishable from one another. It was also found that the results of two or three irradiations on the same fiber at  $10^9$  rads per second appeared identical, but it was decided to maintain the use of fresh fiber for each irradiation at this level.

Before presenting the radiation test results, it is important to mention significant changes in fiber transmission observed during variations of temperature. The greatest change was observed during warmup. As the fiber was heated from room temperature (about 20°C) the detected light output from the fiber dropped steadily until at +125°C it was more than an order of magnitude lower than its starting level. The major cause of this loss in transmission is probably stress produced by expansion of the aluminum reel, even though the fiber was wound on the reel as loosely as possible while maintaining thermal contact. However, other factors such as the expansion of the fiber's protective coating, cannot be ruled out.

As the fibers were cooled below room temperature a drop in signal level was also observed, but not nearly as severe as with increasing temperature, being down on the order of 10 percent at -55°C. In either case, however, once temperature had been reached signal fluctuations were observed as the temperature cycled around its control point. These fluctuations have an important bearing on the accuracy of the steady-state test results. Without the fluctuations the estimated accuracy is  $\pm 1\text{dB}/\text{km}$  and at -55°C and +25°C the fluctuations change this to  $\pm 2\text{dB}/\text{km}$ . At +125°C, as a result of the severe loss in signal, the accuracy is probably reduced to  $\pm 10\text{dB}/\text{km}$ . For the transient tests estimated accuracy is  $\pm 3\text{dB}/\text{km}$  based on the readability of oscilloscope photographs. Because of the short time spans over which the transient measurements were made, the signal variations should not change this. However the loss of signal at +125°C probably reduces the accuracy to  $\pm 6\text{dB}/\text{km}$  due to the decrease in signal to noise ratio.

#### Results of Steady-State Tests

Figure 1 shows the steady-state induced loss as a function of dose measured for fiber WP-2 at -55°C, +25°C and +125°C. Although it was intended to irradiate all the test fibers to 10 Krads, the data at -55°C and +125°C ends at just over 6 Krads. This was due to temporary failure of the linac, and because the fibers had received sufficient dose for purposes of the tests, the irradiation was stopped in order to obtain data on the recovery of induced loss following continuous irrad-

iation. (There was not enough of this fiber available from a single draw to repeat the test.) The interesting features of this data, are the increasing rate of induced loss with temperature and the significant change in slope with increasing dose at +125°C. Figure 2 shows the recovery of induced loss, expressed as a fraction of the loss at the end of irradiation, for this fiber. There is significant recovery only at +125°C. At -55°C, recovery could be followed only for 5 hours due to depletion of the liquid nitrogen. As the temperature increased from -55°C, the loss increased until at +25°C it was 1.2 times the loss at the end of irradiation.

Figure 3 shows the results of the steady-state irradiations of fiber WP-6. The rates of induced loss are significantly less than those for fiber WP-2. The data taken at +125°C does not follow the trend of increasing rate of induced loss with increasing temperature, nor does it show the significant change in slope observed with WP-2. This is probably due to a small temperature excursion near the beginning of the irradiation which may be indicated by the slightly concave portion of the plot near 1 Kilotrad. Also, the data shown for +125°C is the second of two irradiations (a new length of fiber was used for the second irradiation). The data from the first irradiation was not used because the dosimetry showed an unexpected decrease in dose per pulse from the linac. The first set of data did show a significantly higher rate of induced loss at the beginning of the irradiation. Figure 4 shows the recovery of induced loss following irradiation for WP-6. Significant recovery occurs only at +125°C and the rate of recovery is less than for WP-2. Again, when the fiber irradiated at -55°C returned to +25°C the loss increased by a factor of 1.2 times that at the end of irradiation.

Figure 5 shows the results of the steady-state Cobalt 60 irradiations of fiber WP-6. The consistent increase in rate of induced loss with increasing temperature, not seen in the linac data, is clear in this case. Comparison with the linac data shows that the data taken at -55°C are essentially identical and the data at +25°C are very nearly the same. The difference in the data at +125°C is probably due to the high sensitivity of the fiber transmission to small changes in temperature at this temperature. (The control of temperature in the linac irradiation area is somewhat more difficult at +125°C than in the cobalt cell because of a fast-moving air stream required to remove ozone during linac operation).

#### Results of Transient Tests

Figure 6 shows the induced loss as a function of time for fiber WP-2 following a 20 nanosecond,  $2 \times 10^9$  rad/sec pulse from the flash x-ray generator. The induced loss has been normalized to actual dose rate and is presented in units of dB/km per  $10^8$  rads/sec. The reason for this normalization is that the flash x-ray does not necessarily produce the same dose from pulse to pulse. Although the variation in output for a given series of irradiations is only about 10 percent, greater variations can occur over time as the flash x-ray cathode ages. The normalization helps in comparing sets of data by essentially cancelling these variations.

As Figure 6 shows, the amount of transient loss induced in the fiber decreases with increasing temperature, opposite to what was observed in the steady state irradiations. The rate of decay of the induced loss increases with temperature. The actual induced loss at zero time is undoubtedly much greater than the maximum shown by the data. An initial fluorescent pulse (probably Cerenkov radiation)

obscures the loss at early times and, since the fluorescence generated in the fiber has a transit time of about 5 nanoseconds per meter of fiber the true loss is not observable until 400 nanoseconds after the radiation pulse (5 nanoseconds per meter times 80 meters of fiber including leads). At all three temperatures the chart recorder showed a residual loss out to 70 seconds of the order of 0.1 dB/km per  $10^8$  rads per second, which is below the estimated accuracy of the measurement.

For the nominal  $10^8$  rads/sec irradiations (actual dose-rate  $1.6 \times 10^8$  rads/sec) the observed induced losses were close to the limit of measurement. No induced loss was observable at  $+125^\circ\text{C}$ . At  $+25^\circ\text{C}$  the maximum induced loss was approximately 2 dB/km per  $10^8$  rads/sec and at  $-55^\circ\text{C}$  it was about 4 dB/km per  $10^8$  rads/sec. Loss was detectable beyond the maximum only at  $-55^\circ\text{C}$ , and this appeared to go to zero at 30  $\mu\text{sec}$  after the x-ray burst.

Figure 7 shows the response of fiber WP-6 to a nominal  $10^9$  rads/sec (actual dose rate  $1.1 \times 10^9$  rads/sec) x-ray burst. The results are similar in form to those obtained for WP-2, but the normalized induced losses are about twice those for WP-2 and the rate of recovery is slower.

The  $10^8$  rad/sec (actual dose rate  $1.3 \times 10^8$  rads/sec) exposure showed induced losses near the measurable limit but greater than those for WP-2. At  $-55^\circ\text{C}$  the maximum observed loss was 8 dB/km per  $10^8$  rads/sec and loss was evident to 7 milliseconds. At  $+25^\circ\text{C}$  the maximum loss was about 3.5 dB/km per  $10^8$  rads/sec with no loss detectable beyond 5 microseconds. At  $+125^\circ\text{C}$  a maximum loss of 1 dB/km per  $10^8$  rads/sec only was seen.

### Summary

The results of the tests may be summarized as follows:

1. Under steady-state irradiation the rate of induced loss as a function of dose increases with increasing temperature.
2. Under transient radiation conditions the maximum induced loss decreases with increasing temperature while the rate of recovery increases with temperature.
3. Significant recovery of induced loss following steady-state irradiation occurs only at higher temperatures.
4. The use of a linear accelerator, a pulsed radiation source, to simulate steady-state irradiation is valid, assuming the differences between the linac and Cobalt-60 results observed at  $+125^\circ\text{C}$  are due to the sensitivity of the fiber transmission (in the test configuration used) to small changes in temperature.
5. Following steady-state irradiation at  $-55^\circ\text{C}$ , the radiation induced loss increases as the temperature is increased. When the fiber temperature returns to  $+25^\circ\text{C}$ , the loss is about the same as if the fiber had been irradiated at that temperature.
6. An increased percentage of germanium in the fiber core results in a decrease in the rate of induced loss as a function of dose under steady-state

irradiation and an increase in induced loss under transient irradiation.

The tests results reported here are for specific fiber compositions. The differences observed between the radiation responses of fibers WP-2 and WP-6 show that the results should not be generalized as representative of all germanium-phosphosilicate fibers.

RESPONSE TO 10 Mev LINAC X-RAYS  
FIBER: WP-2

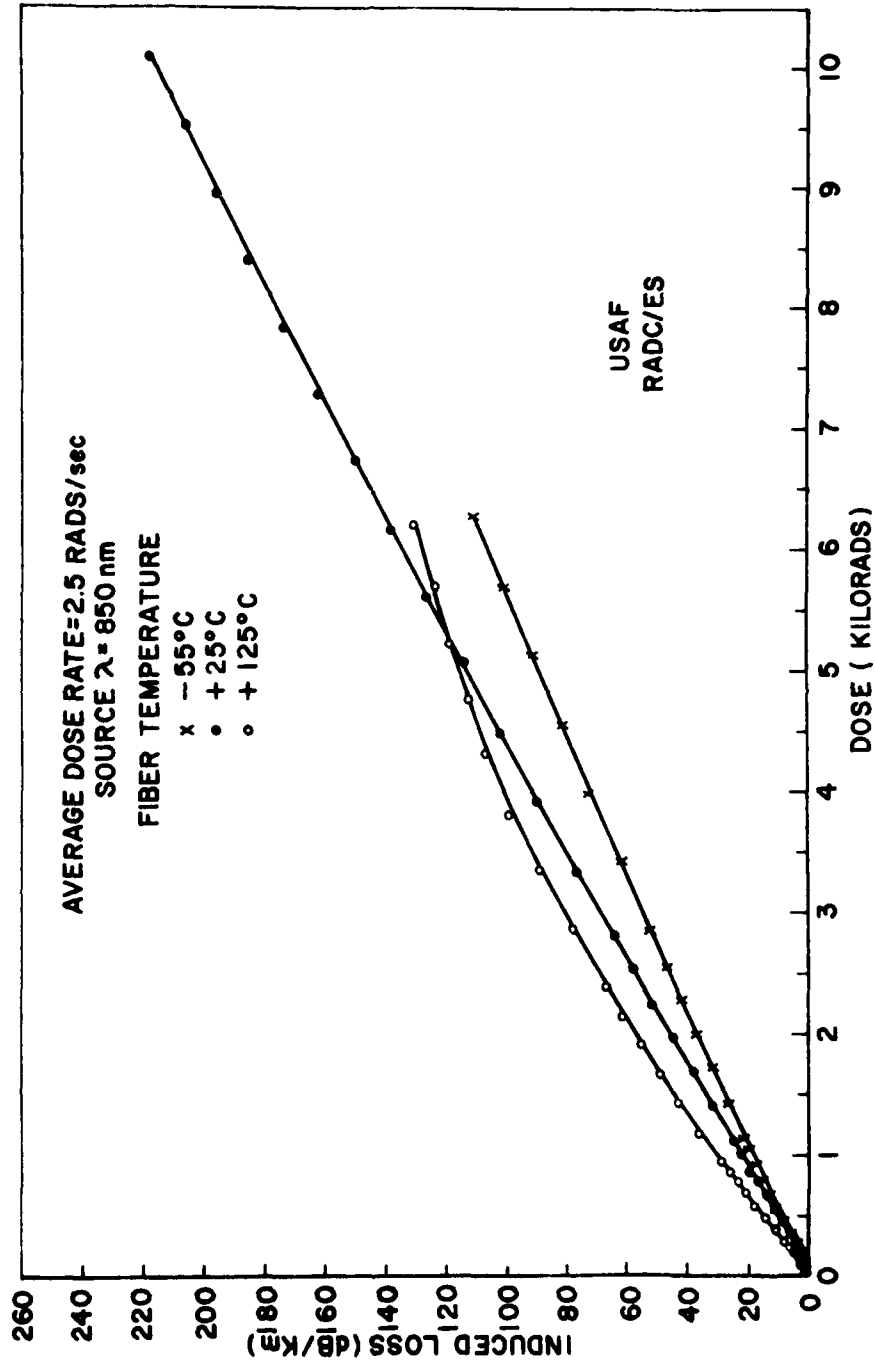


Figure 1

RECOVERY OF RADIATION INDUCED LOSS  
FIBER: WP-2

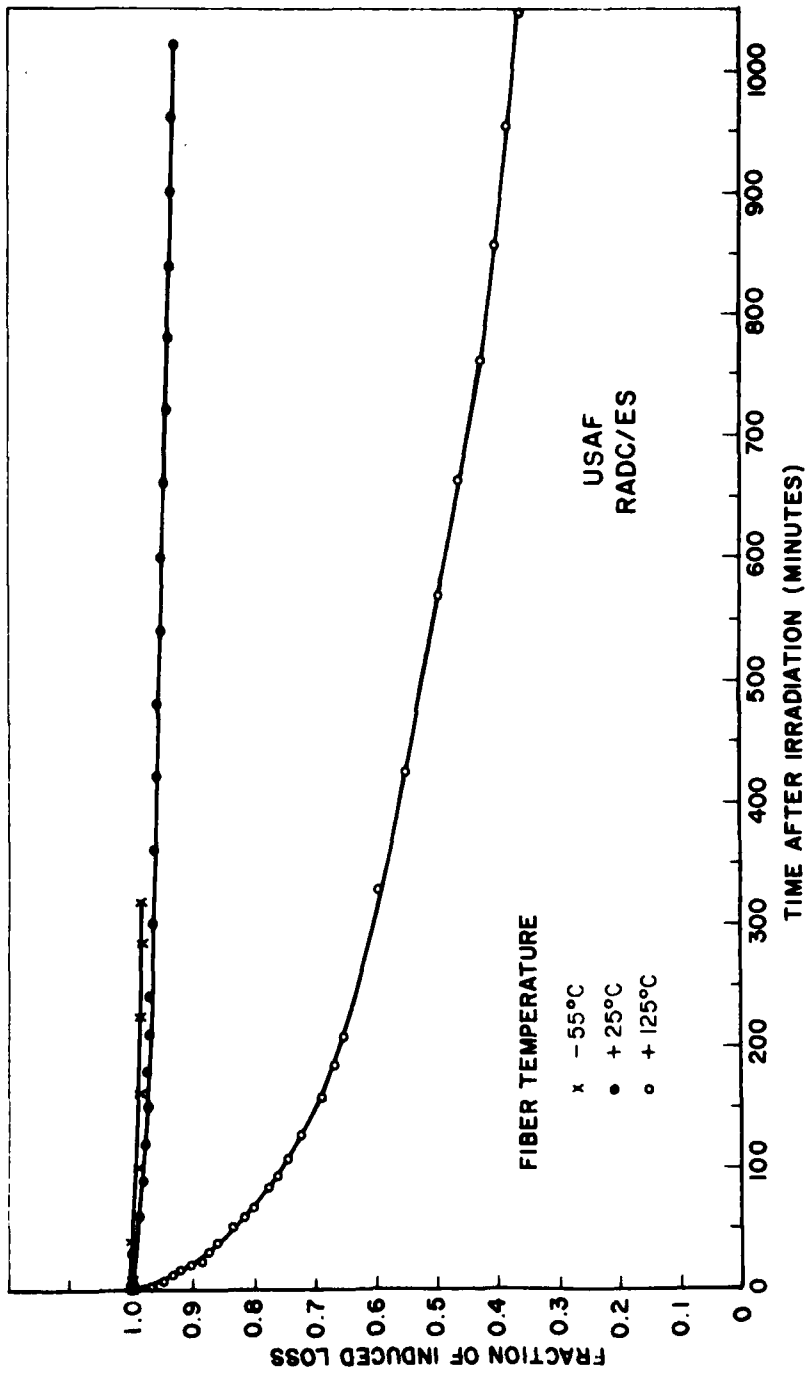


Figure 2

RESPONSE TO 10 Mev LINAC X-RAYS  
FIBER: WP-6

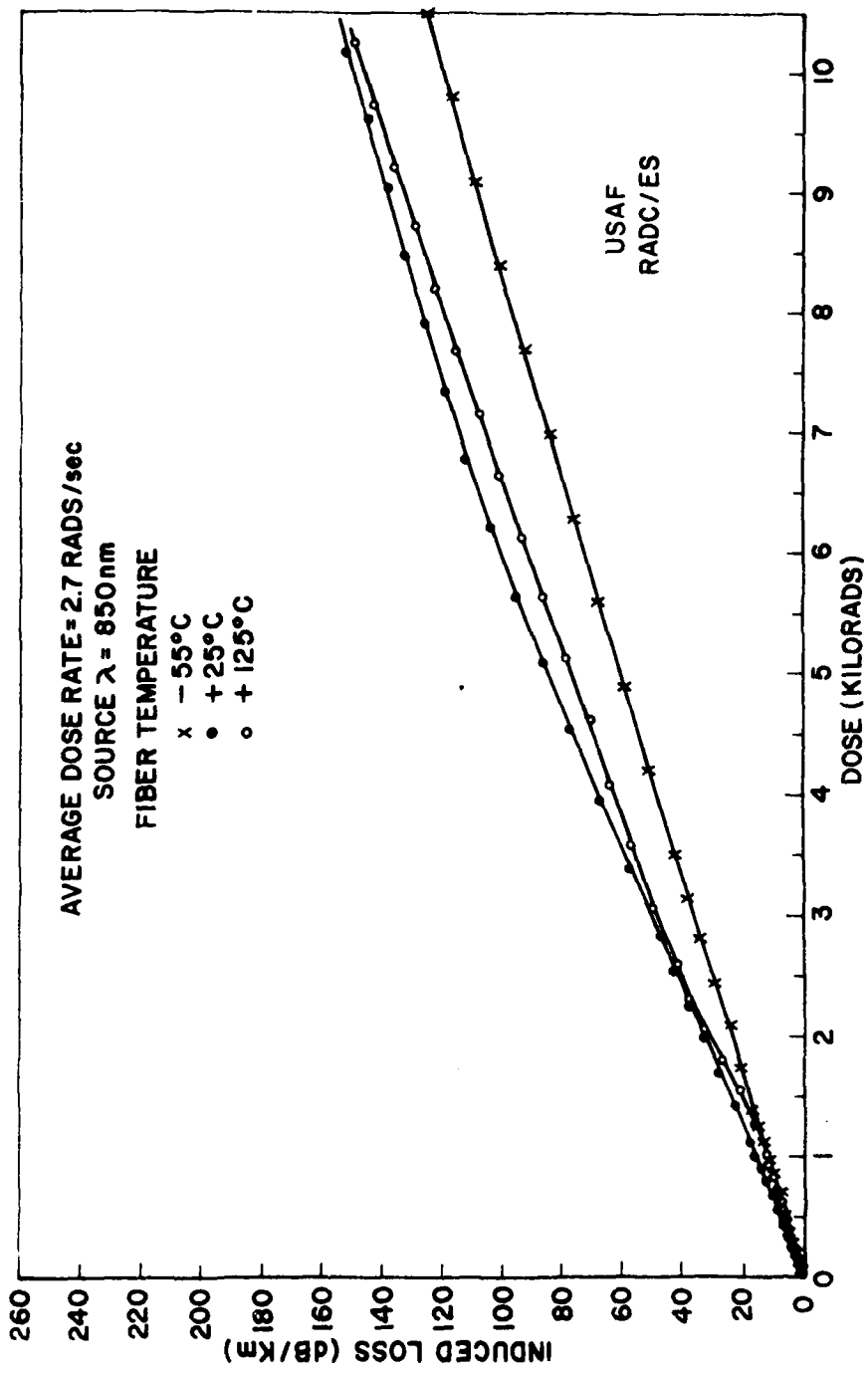


Figure 3

RECOVERY OF RADIATION INDUCED LOSS  
FIBER: WP-6

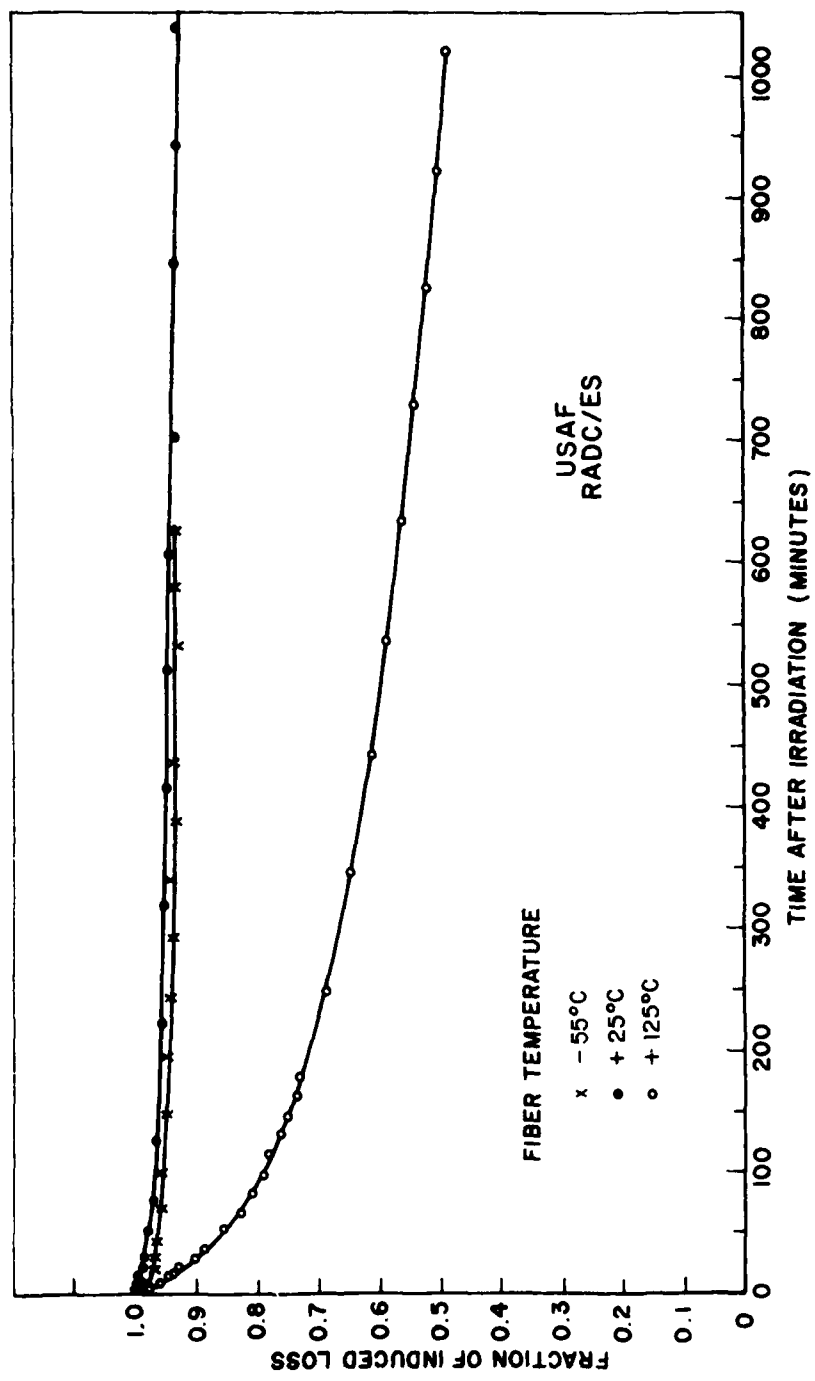


Figure 4

RESPONSE TO CO-60 RADIATION  
FIBER: WP-6

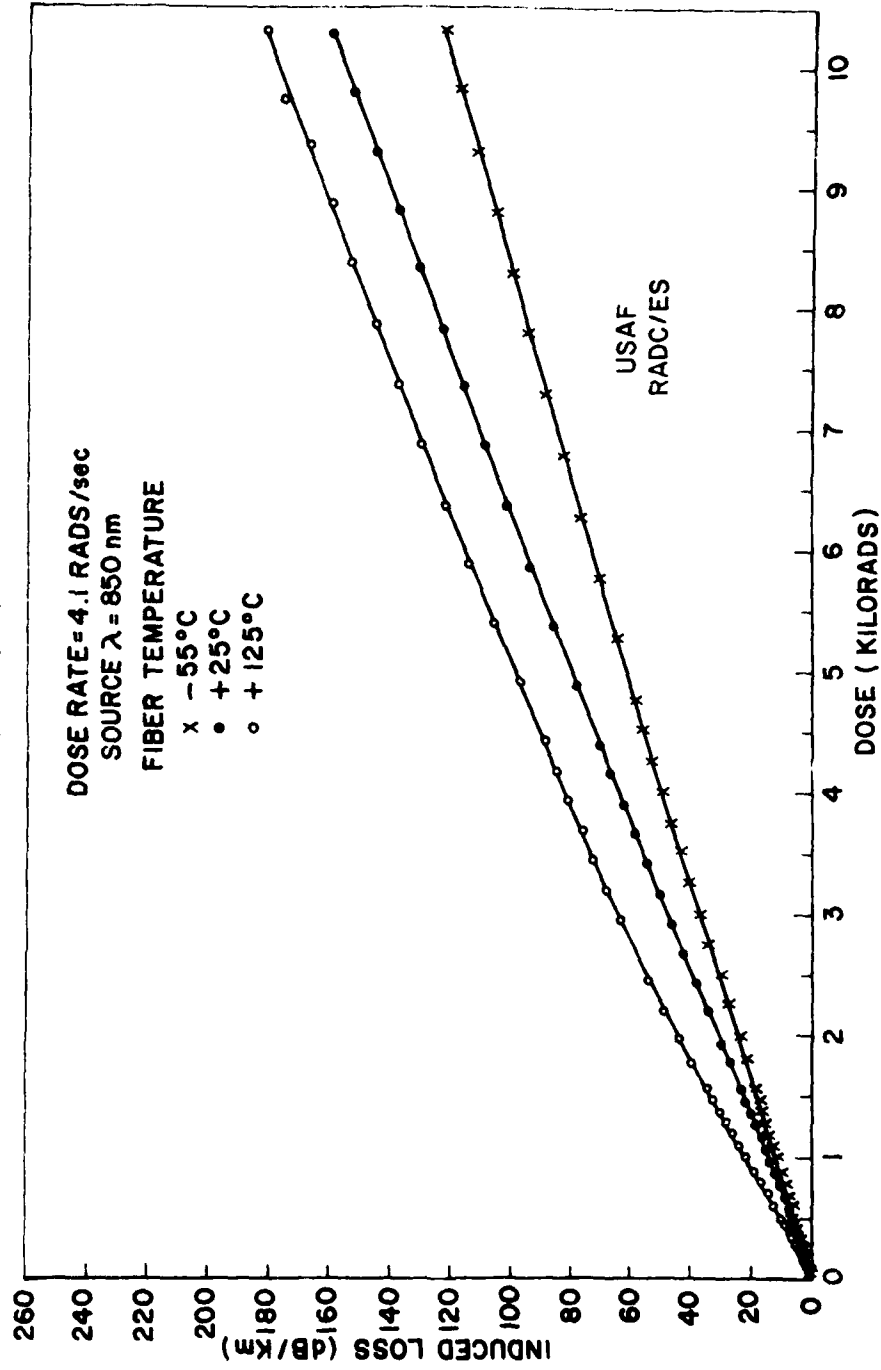


Figure 5

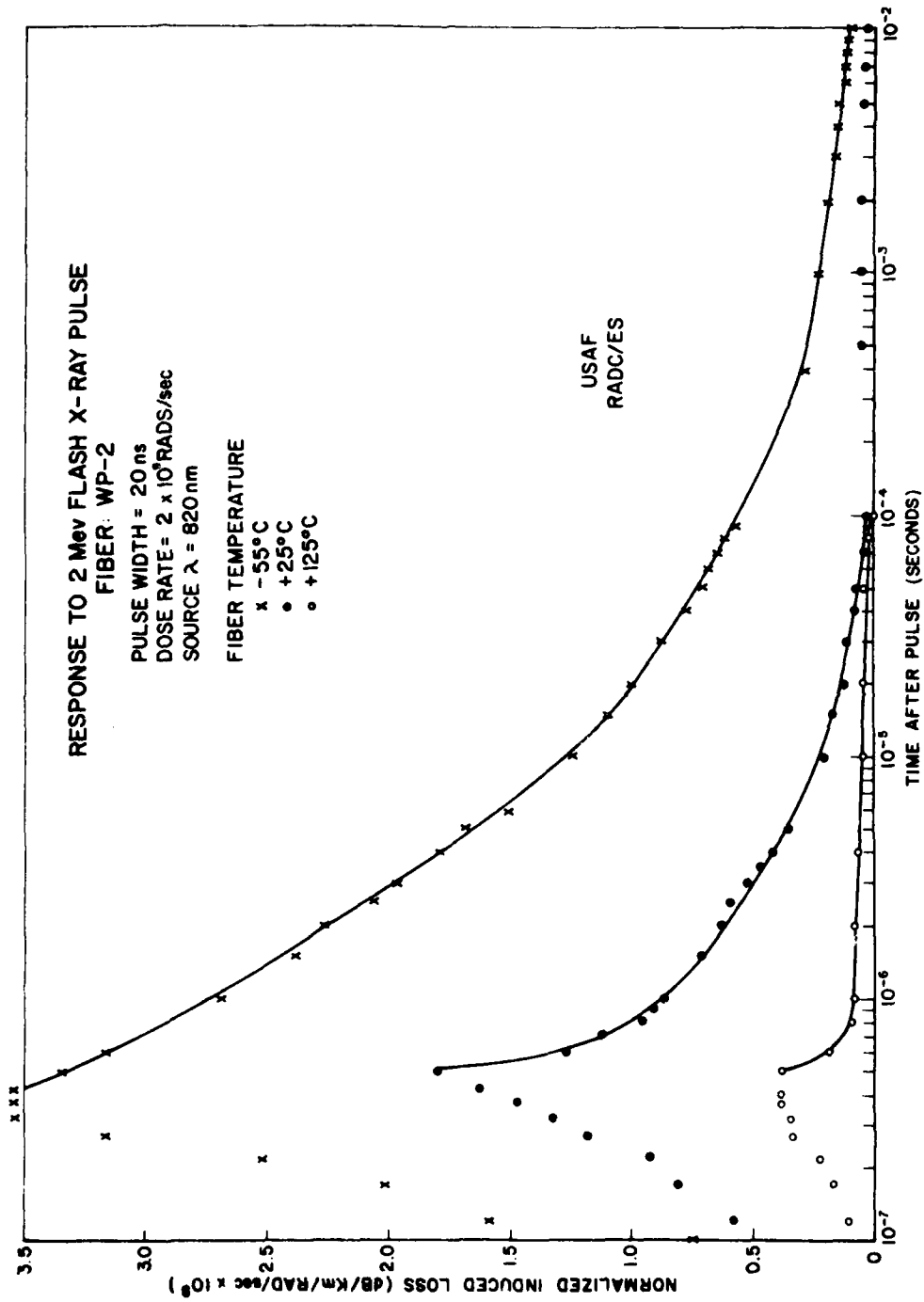


Figure 6

AD-A101 430

GALILEO ELECTRO-OPTICS CORP STURBRIDGE MA  
RADIATION HARD FIBER OPTICS.(U)

MAY 81 R E JAEGER, M ASLAMI

F/6 20/6

F19628-78-C-0099

NL

UNCLASSIFIED

RADC-TR-81-69

2 x 2  
406  
17430



END  
DATA  
FILED  
8-81  
DTIC

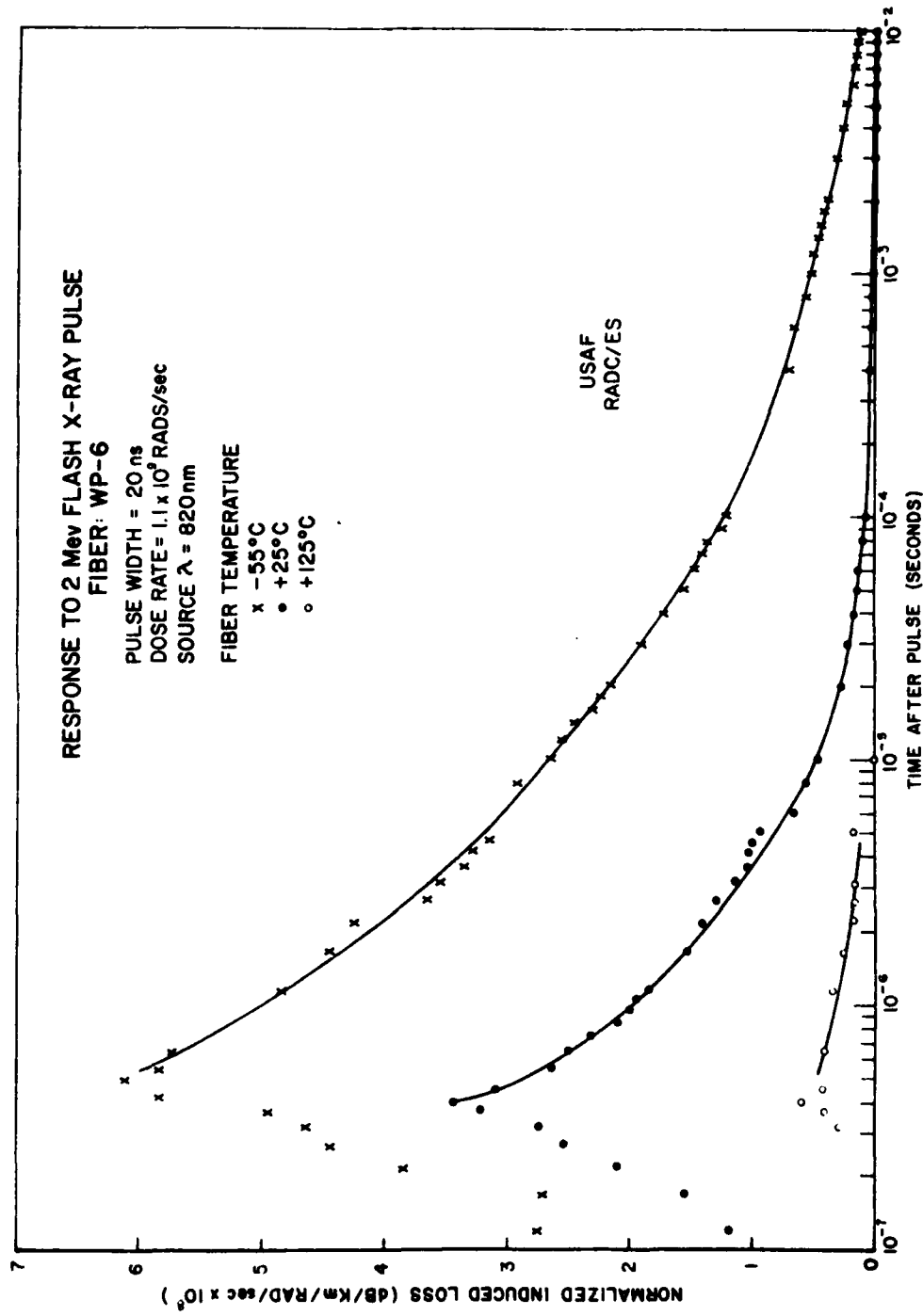


Figure 7

MISSION  
of  
Rome Air Development Center

RADC plans and executes research, development, test and selected acquisition programs in support of Command, Control Communications and Intelligence (C<sup>3</sup>I) activities. Technical and engineering support within areas of technical competence is provided to ESD Program Offices (POs) and other ESD elements. The principal technical mission areas are communications, electromagnetic guidance and control, surveillance of ground and aerospace objects, intelligence data collection and handling, information system technology, ionospheric propagation, solid state sciences, microwave physics and electronic reliability, maintainability and compatibility.

**DATE:  
ILME**